Memoirs of the Faculty of Engineering, Nagoya University
Vol. 30, No. 1. (1978)

UNSTEADY HEAT CONDUCTION ACCOMPANIED BY AN ENDOTHERMIC SOLID REACTION

SACHIO SUGIYAMA and MASANOBU HASATANI

Department of Chemical Engineering

(Received May 31, 1978)

CONTENTS

Abstract

Introducing the concept of the overall specific heat, a basic equation for an unsteady heat conduction accompanied by an endothermic solid reaction was reduced to the form of an ordinary unsteady heat conduction equation with variable thermal properties. For crystal transformation and thermal decomposition on which a mass transfer rate has only a little and limited effect, the method of modelling the relation between the overall specific heat and temperature was deduced theoretically based on the simplified intrinsic reaction kinetics.

A hot wire method was discussed to avoid appreciable errors caused by an end effect and a thermal-contact resistance and to measure the thermal conductivities of a reactant and a product solid at elevated temperatures.

By applying the principles of a differential thermal analysis, a new measurement method was developed to qualify the thermal conductivity with reaction. It was shown from the results of the measurements that the temporary disorder or disintegration of a crystal lattice caused intrinsically by the reaction had a controlling effect on the thermal conductivity with reaction and then that the thermal conductivity with reaction had a smaller value than those in the non-reacting states.

Taking account of the results from the above measurements and from the precise evaluations of thermal properties, the numerical solutions of the basic equation were presented not only for an one-stage endothermic solid reaction but also for a two-or a multi-stage reaction, and the powerful applicabilities of the overall specific heat and the thermal conductivity with reaction to the engineering problems were demonstrated experimentally.

1. Introduction

Chemical processes involving a solid reaction have a great need over a wide range of industrial fields. Not only in a chemical industry but also in other manufacturing industries like a metallurgical, an iron and steel, an insulating and refractory material, and a nuclear furnace material industry, a solid reaction is directly or indirectly involved in a heart core of a sequence of the production steps in those processes. Recently, also in the area of newly developing technologies concerning an energy problem and a high-temperature thermal protection problem, a new need of a solid reaction is rapidly increasing. A reversible endothermic and exothermic cycle of a solid reaction is offering one of the promising solutions to a heat recovery or a heat storage problem, and a thermal protector formed out of an endothermic solid reactant has also been recognized to be one of the qualified protectors, owing to its high protection ability and the easiness of its control.

For the optimal design and control of those processes, one of the key factors is to find the conditions under which the processes can be operated thermally effectively. Especially, in case of an endothermic reaction, the characteristic of heat transfer in the processes often directly relates to the conditions of the optimal

design and control. As is well known, in a solid reaction, the overall reaction rate is usually affected by heat and mass transfer rates as well as by an intrinsic reaction rate. The general concept of the relationship between the overall reaction rate and these three rate-affecting parameters is extremely complicated, and an effect of each parameter differs from each other depending not only on the mode of reaction but also on the operating conditions employed. Because of such difficulties in the problem, although a number of theoretical approaches have been reported so far, those involve, if any, some of the key assumptions. One of the most successful key assumptions in those approaches is the assumption of 'Pseudo Steady State'. So long as heat transfer is not concerned, this key assumption would be highly useful to reduce the mathematical difficulties in the problem in spite of the unsteadiness of a solid reaction itself. However, in case where heat transfer is concerned, the assumption of 'Pseudo Steady State' is not necessarily valid. This is principally due to a relatively large heat capacity of a solid concerned. Thus, for a heat transfer analysis accompanied by a solid reaction, in general, an unsteady state treatment is essentially required.

The purpose of the present study is to develop a simple and useful mathematical model for an unsteady heat conduction problem accompanied by an endothermic solid reaction which would be affected more largely by the heat transfer characteristic in the processes. The reactions dealt with in the present study are crystal transformation and thermal decomposition, expressed in the forms,

crystal transformation:

$$\mathbf{A}\ \text{(reactant crystal)} \rightleftarrows \mathbf{P}\ \text{(product crystal)} \tag{1}$$

thermal decomposition:

$$a\mathbf{A}\ \text{(solid reactant)} \rightleftarrows p\mathbf{P}\ \text{(product solid)} + q\mathbf{Q}\ \text{(product gas or liquid)}$$

As is seen from Equation (1), mass transfer has no effect on crystal transformation, and only an indirect and limited effect on thermal decomposition. Further, these reactions usually take place in the distinctive and narrow temperature range with the relatively large endothermic heat. Therefore, these reactions have also a suitable characteristic to discuss precisely the relationship between the unsteady heat conduction and the overall reaction kinetics by applying an appropriate technique to reduce the mathematical difficulties.

The mathematical model developed in the present study is called the 'overall specific heat' model. In this model, the endothermic heat of reaction is involved in the overall specific heat defined in the range of reaction temperature, and the basic unsteady heat conduction equations are solved as a variable thermal property problem.

Before solving the basic equations, we need a precise evaluation or measurement of the thermal properties concerned. In a solid reaction, in general, not only the change of the macroscopic structural properties of the solid (such as the void fraction) but also the rearrangement of the micro-crystal structure may take place in the course of the reaction. Therefore, the thermal properties, especially the thermal conductivity, may have somewhat big differences between in the pre- and in the post-reaction states, and at the same time the thermal conductivity during the period when the reaction is occuring would be expected to differ from those in the non-reaction states (the pre- and the post-reaction states). A consideration on those matters also are involved in the present study.

2. The Concept of Overall Specific Heat[1, 2]

The basic equation of unsteady heat conduction in a solid particle (assumed to be a sphere) accompanied by a solid reaction can be, in the general form, written as

$$c_p\rho\left(\frac{\partial t}{\partial \theta}\right)=\frac{1}{r^2}\frac{\partial}{\partial r}\left(\lambda r^2\frac{\partial t}{\partial r}\right)-H\rho_1\left(\frac{\partial k}{\partial \theta}\right) \tag{2}$$

where H and k denote a heat of reaction per unit mass and a fraction of reaction (a conversion), respectively, and the term of $(\partial k/\partial\theta)$ corresponds to an intrinsic reaction rate.

The intrinsic rate expression of an usual solid reaction may be so complicated as

$$\frac{\partial k}{\partial \theta}=f(k,\ t,\ c_f) \tag{3}$$

where c_f is a concentration of a gaseous or liquid reactant. On crystal transformation and thermal decomposition, however, the concentration, c_f, has only a limited effect from the above-mentioned reason. Therefore, we may simplify the intrinsic rate expression of these reactions, assuming a first order-reaction with respect to a solid reactant, as

$$\frac{\partial k}{\partial \theta}=f(t)(1-k) \tag{4}$$

Integrating Equation (4), we obtain

$$k=1-exp\left[-\int f(t)\,d\theta\right] \tag{4}'$$

Since the temperature in the solid, t, is a function of a reaction time, θ, we get

$$k=g(t) \tag{5}$$

Thus

$$\left(\frac{\partial k}{\partial \theta}\right)=g'(t)\left(\frac{\partial t}{\partial \theta}\right) \tag{6}$$

Substituting Equation (6) into Equation (2), we obtain

$$\left[c_p+Hg'(t)(\rho_1/\rho)\right]\rho\left(\frac{\partial t}{\partial \theta}\right)=\frac{1}{r^2}\frac{\partial}{\partial r}\left(\lambda r^2\frac{\partial t}{\partial r}\right) \tag{7}$$

Putting

$$C_p(t)=c_p+Hg'(t)(\rho_1/\rho) \tag{8}$$

Equation (2) can be reduced to the ordinary form of the unsteady heat conduction equation in a sphere:

$$C_p(t)\rho\left(\frac{\partial t}{\partial \theta}\right)=\frac{1}{r^2}\frac{\partial}{\partial r}\left(\lambda r^2\frac{\partial t}{\partial r}\right) \tag{9}$$

$C_p(t)$ in Equation (9) is the overall specific heat involving the heat of reaction. Now, we have assumed k to be a function of temperature only. If a temperature-function, $f(t)$, increases rapidly above a certain temperature characterized by the reaction, this assumption would be expected to be sufficiently valid.

When we consider a two- or a multi-stage reaction, Equations (2) and (4) are rewritten as

$$c_p\rho\left(\frac{\partial t}{\partial \theta}\right)=\frac{1}{r^2}\frac{\partial}{\partial r}\left(\lambda r^2\frac{\partial t}{\partial r}\right)-H_1\rho_1\left(\frac{\partial k_1}{\partial \theta}\right)-H_2\rho_2\left(\frac{\partial k_2}{\partial \theta}\right)-\cdots \tag{2}'$$

$$\frac{\partial k_1}{\partial \theta}=f_1(t)(1-k_1),\quad \frac{\partial k_2}{\partial \theta}=f_2(t)(1-k_2),\ \cdots \tag{4}''$$

or when k_1, k_2, $\cdots$ have to do with each other, Equation (4)'' becomes

$$\frac{\partial k_1}{\partial \theta}=f_1(t,\ k_1,\ k_2,\ \cdots),\quad \frac{\partial k_2}{\partial \theta}=f_2(t,\ k_1,\ k_2,\ \cdots),\ \cdots \tag{4}'''$$

In such cases, taking account of the complexity of dealing with these equations, the assumptions of $k_1=g_1(t)$, $k_2=g_2(t)$, $\cdots$, and of $C_p(t)=c_p+H_1g_1'(t)(\rho_1/\rho)+H_2g_2'(t)(\rho_2/\rho)+\cdots$ are considered more practical without an appreciable error. Hence, we can also apply Equation (9) to the two- or the multi-stage reaction.

Since it is possible to obtain the overall specific heat-temperature relation in a reasonable way from the overall kinetic data of the reaction or at least based on a trial-and-error method, we can get the solution of the unsteady heat conduction problem accompanied by the endothermic solid reaction like crystal transformation and thermal decomposition from Equation (9) by an appropriate numerical method. A few typical examples of the overall specific heat-temperature relations are shown in Fig. 1.

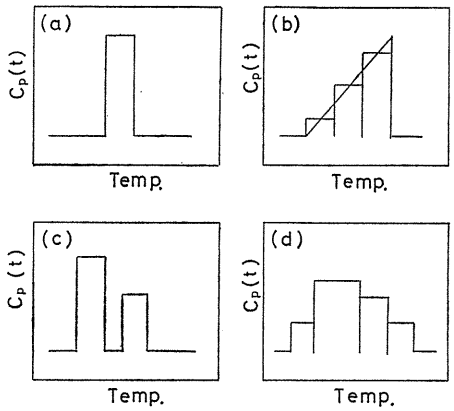

Fig. 1. Typical examples of the overall specific heat-temperature relations.

3. Thermal Conductivity Measurements

3. 1. Thermal Conductivity Measurement in the Non-Reaction States by a Hot Wire Method[3]

A hot wire method was employed to measure the thermal conductivities of the solid materials concerned in the present study in the non-reaction states.

From a given time, an electric current is applied through a thin straight wire, placed in the homogeneous material of which the thermal conductivity is to be measured. The electrical heat produced at a constant rate in the wire causes a cylindrical temperature field in the material. The rise in the surface temperature of the wire is dependent on the thermal properties of this material. This is the principle of measuring a thermal conductivity by a hot wire method. The applicability of this method has already been discussed extensively, and it has been qualified that this method is usually useful for materials of lower thermal conductivity and is more advantageous than an usual steady state method because the measurement can be carried out during shorter elapsed time even at elevated temperatures.[4, 5]

Such advantages of this method would profit the thermal conductivity measurement concerned. However, in this method, the measured data are sometimes badly affected by an end effect, but the relation between material dimensions and an end effect has not been discussed sufficiently.[6] Thus the discussion in this section intends to deduce its relation theoretically and to demonstrate it in the measurement for a standard material.

3. 1. 1. Theoretical Consideration on an End Effect

A thin straight wire, used as an electrical heater, is immersed along the axis of a cylindrical material, as shown in Fig. 2. The outer surface temperature of the material is maintained at a given initial temperature, t_0, throughout the measurement. Since the wire is usually very thin and made of a good thermal conductor, the radial temperature distribution in the wire is assumed to be negligibly small. A constant heat flow, Q_0, is produced in the wire. A thermal contact-resistance may exist at the boundary between the wire and the material. Thus, the unsteady temperature profile in the material would be determined by the following Equation (10) with the boundary conditions (11) through (14);

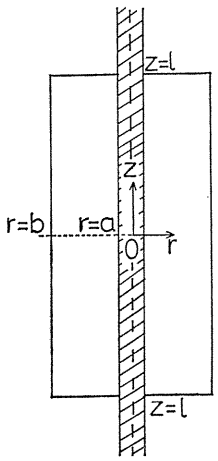

Fig. 2. A coordinate system of a hot wire method.

$$\frac{1}{r}\frac{\partial}{\partial r}\left(r\frac{\partial t}{\partial r}\right)+\frac{\partial^2 t}{\partial z^2}-\frac{1}{\alpha}\frac{\partial t}{\partial \theta}=0 \qquad (10)$$

$$\theta=0, \quad 0\leq r\leq b, \quad -l\leq z\leq l; \quad t=t_0 \qquad (11)$$

$$\theta\geq 0, \quad z=\pm l; \quad t=t_0 \qquad (12)$$

$$r=b\,; \qquad t=t_0 \tag{13}$$

$$r=a\,; \qquad -\lambda\left(\frac{\partial t}{\partial r}\right)=h_{cr}(t_w-t_a) \tag{14}$$

The unsteady axial temperature profile in the wire is also expressed in the form of Equation (15) with the initial condition (16).

$$\frac{\partial^2 t_w}{\partial z^2}-\frac{2h_{cr}}{a\lambda_w}(t_w-t_a)-\frac{1}{\alpha_w}\frac{\partial t_w}{\partial \theta}+\frac{Q_0}{\lambda_w}=0 \tag{15}$$

$$\theta=0, \quad -l\leq z\leq l\,; \quad t_w=t_0 \tag{16}$$

Using the non-dimensional variables of $t^*=(t-t_0)/t_0$, $t_w^*=(t_w-t_0)/t_0$, $r^*=r/a$, $z^*=z/a$, and $\tau=\alpha\theta/a^2$, the above equations and the boundary conditions are re-written as follows;

(For the material)

$$\frac{1}{r^*}\frac{\partial}{\partial r^*}\left(r^*\frac{\partial t^*}{\partial r^*}\right)+\frac{\partial^2 t^*}{\partial z^{*2}}-\frac{\partial t^*}{\partial \tau}=0 \tag{10}'$$

$$\tau=0, \quad 0\leq r^*\leq b/a, \quad -l/a\leq z^*\leq l/a\,; \quad t^*=0 \tag{11}'$$

$$\tau\leq 0, \quad z^*=\pm l/a\,; \qquad t^*=0 \tag{12}'$$

$$r^*=b/a\,; \qquad t^*=0 \tag{13}'$$

$$r^*=1\,; \qquad \frac{\partial t^*}{\partial r^*}=-\frac{ah_{cr}}{\lambda}(t_w^*-t_a^*) \tag{14}'$$

(For the wire)

$$\frac{\partial^2 t_w^*}{\partial z^{*2}}-\frac{2h_{cr}a}{\lambda_w}(t_h^*-t_a^*)-\frac{\alpha}{\alpha_w}\frac{\partial t^*}{\partial \tau}+\frac{Q_0}{\lambda_w}\frac{a^2}{t_0}=0 \tag{15}'$$

$$\tau=0, \quad -l/a\leq z^*\leq l/a\,; \quad t_w^*=0 \tag{16}'$$

From Equations (11)′ through (16)′, the Laplace transformation, T^* (1, 0, p), of the surface temperature, t^* (1, 0, τ) at the center ($r^*=1$, $z^*=0$) of the wire is obtained as

$$T^*(1,\ 0,\ p)=\frac{Q_0a^2}{2\lambda t_0}\frac{1}{p}\sum_{n=0}^{\infty}\{4(-1)^n/(2n+1)\}\mathrm{F}_0\Big/\left[\frac{\mathrm{F}_0}{2\lambda/\lambda_w}\left[\left\{\frac{(2n+1)\pi a}{2l}\right\}^2+\frac{\alpha}{\alpha_w}p\right]-\mathrm{F}_1\sigma_n\left[1+\frac{\lambda_w}{2ah_{cr}}\left\{\frac{(2n+1)\pi a}{2}\right\}^2+\frac{\alpha}{\alpha_w}p\right]\right] \tag{17}$$

where $\mathrm{F}_0=\mathrm{I}_0(\sigma_n)\mathrm{K}_0(\sigma_n b/a)-\mathrm{I}_0(\sigma_n b/a)\mathrm{K}_0(\sigma_n)$,
$\mathrm{F}_1=\mathrm{I}_1(\sigma_n)\mathrm{K}_0(\sigma_n b/a)+\mathrm{I}_0(\sigma_n b/a)\mathrm{K}_1(\sigma_n)$, and $\sigma_n=[p+\{(2n+1)\pi a/2l\}^2]^{1/2}$

1) Infinite Material

In an infinite material, the transform T^* ($b\to\infty$, $l\to\infty$) would be obtained from Equation (17) by substituting $b=\infty$ and $l=\infty$ into the equation as

$$T^*(b\to\infty,\ l\to\infty)=-\frac{Q_0a^2}{2\lambda t_0}\frac{1}{p}\frac{\mathrm{K}_0(\sqrt{p})}{Ap\mathrm{K}_0(\sqrt{p})+(1+Bp)\sqrt{p}\mathrm{K}_1(\sqrt{p})} \tag{18}$$

where $A=c_{pw}\rho_w/2c_p\rho$ and $B=(\lambda/2ah_{cr})(c_{pw}\rho_w/c_p\rho)$. Now, if the elapsed time of the measurement is so large that the limitation, $\tau\gg1$, is valid enough in Equation (18), $T^*(b\to\infty,\ l\to\infty)$ may be approximately expanded in ascending series of a parameter, p, taking account of $p\ll1$;

$$T^*(b\to\infty,\ l\to\infty)=-\frac{Q_0a^2}{2\lambda t_0}\frac{1}{p}\left[\frac{1}{2}ln\frac{c^2p}{4}+\frac{p}{4}\left\{(1-2B)ln\frac{c^2p}{4}-\frac{1-2A}{2}\left(ln\frac{c^2p}{4}\right)^2-1\right\}+O(p^2)\right] \tag{19}$$

where $ln\ C=0.5722$ (the Euler's constant)

From the inversion theorem of the Laplace transformation, the surface temperature, $t_w^*(\infty,\ \infty,\ \tau)$, becomes

$$t_w^*(\infty,\ \infty,\ \tau)=\frac{Q_0a^2}{2\lambda t_0}\left[\frac{1}{2}ln\frac{4\tau}{c}+\frac{1}{4\tau}\left\{(1-2B)+(1-2A)ln\frac{4\tau}{c}\right\}+O(1/\tau^2)\right] \tag{20}$$

Again, if the elapsed time, τ, is so large that the second term of the right side of Equation (20) also is insignificant in magnitude, the thermal conductivity may be determined graphically from the slope of the line, by fitting a straight line to the plot of $t_w^*(\infty,\ \infty,\ \tau)$ against $ln(\tau)$. To estimate such a critical value of τ, the magnitudes of A and B must be known. A is expressed as $c_{pw}\rho_w/2c_p\rho$, using the physical properties of the wire and the material. Generally, the relations of $c_{pw}<c_p$ and $\rho_w>\rho$ are valid, and the value of A is likely to be nearly unity. In the present measurement, a constantan wire and polyethylene were employed as a heater and a standard material to examine an end effect. In this case, the value of A becomes 0.84. Then $(1-2A)\simeq-1$. On the other hand, B is expressed as $\lambda A/ah_{cr}$. If the thermal contact-resistance, $1/h_{cr}$, becomes larger and larger, the B-value also becomes significant. When the thermal contact-resistance is small and insignificant, namely $B\simeq0$, the critical value of τ becomes, within an error of 1 %,

$$\tau\gtrsim40 \tag{21}$$

For the significant value of $1/h_{cr}$, the critical value of τ may be estimated by taking account of the time lag by the thermal contact-resistance. This can be shown by putting $\tau+\tau_0$ instead of τ in Equation (20);

$$t_w^*(\infty,\ \infty,\ \tau)=\frac{Q_0a^2}{4\lambda t_0}\left[ln\frac{4\tau}{c}+ln\left(1+\frac{\tau_0}{\tau}\right)+\frac{1}{2(\tau+\tau_0)}\left\{(1-2B)+(1-2A)ln\frac{4\tau}{c}\left(1+\frac{\tau_0}{\tau}\right)\right\}+O\left\{\frac{1}{(\tau+\tau_0)^2}\right\}\right]$$

$$=\frac{Q_0a^2}{4\lambda t_0}\left[ln\frac{4\tau}{c}+\frac{1}{2\tau}\left\{2\tau_0+(1-2B)+(1-2A)ln\frac{4\tau}{c}\right\}+O\left(\frac{1}{\tau^2}\right)\right] \tag{22}$$

If τ_0 is chosen so as to satisfy the equation

$$2\tau_0+(1-2B)+(1-2A)ln(4\tau^*/C)=0 \tag{23}$$

Equation (22) becomes

$$t_w^*(\infty,\ \infty,\ \tau)=\frac{Q_0a^2}{4\lambda t_0}\left[ln\frac{4\tau}{c}+\frac{1}{2\tau}(1-2A)ln\frac{\tau}{\tau^*}+O\left(\frac{1}{\tau^2}\right)\right] \tag{24}$$

τ^* may be preferably determined by using the relation $\tau^*=(\tau_1\cdot\tau_2)^{1/2}$ deduced from $ln(\tau^*)=(ln\tau_1+ln\tau_2)/2$, where τ_1 and τ_2 are the elapsed time at the beginning and the end of the experimental data needed to determine the thermal conductivity. From Equation (24), the critical value of τ becomes, within an error of 1 %,

$$\tau\geq 20 \quad or \quad t\geq 20a^2/\alpha \tag{25}$$

From the above result, the surface temperature, t_w^* $(\infty,\ \infty,\ \tau)$, may be expressed as

$$t_w^*(\infty,\ \infty,\ \tau)=\frac{Q_0a^2}{4\lambda t_0}ln\frac{4(\tau+\tau_0)}{c} \tag{26}$$

The time lag, τ_0, may be determined by Equation (23), but is best determined experimentally. The reciprocal of the derivative with respect to time in Equation (26) is

$$\left(\frac{\partial t_w^*}{\partial\theta}\right)^{-1}=\left(\frac{4\lambda t_0}{Q_0a^2}\right)(\theta+\theta_0) \tag{27}$$

If we plot $(\partial t_w^*/\partial\theta)^{-1}$ against time, θ, again we find a straight line with a slope $(4\lambda t_0/Q_0a^2)$. The axis $(\partial t_w^*/\partial\theta)^{-1}=0$ cuts this straight line at $-\theta_0$. We do not use this line to determine λ, since by graphical differentiation we get an inadmissible spread of the points. We use it only to determine θ_0. Then τ_0 is given as the non-dimensional representation of θ_0.

2) Semi-infinite Material $(a\leq r\leq b,\ l\to\infty)$

Let us consider how large the radius of the material must be to obtain the thermal conductivity, λ, by the same procedure as that in an infinite material. In this case, Equation (17) becomes, taking account of $l\to\infty$.

$$T^*(b<\infty,\ l\to\infty)=\frac{Q_0a^2}{2\lambda t_0}\frac{1}{p}\left\{\frac{F_0}{ApF_0-(1+Bp)\sqrt{p}F_1}\right\} \tag{28}$$

To obtain a large time solution, the transform T^* $(b,\ \infty)$ is expanded in ascending powers of $\sqrt{p}$ and $\sqrt{p}b/a$ as follows, taking account of $\sqrt{p}\ll 1$ and $\sqrt{p}b/a\ll 1$;

$$T^*(b,\ \infty)=\frac{Q_0a^2}{2\lambda t_0}\frac{1}{p}\left[ln\frac{b}{a}+\frac{p}{4}\left\{\frac{1-2A}{2}\left(ln\frac{b}{a}\right)^2+(2-4B)ln\left(\frac{b}{a}\right)\right.\right.$$

$$\left.\left.+\left(1-\frac{b^2}{a^2}\right)\right\}+O(p^2)\right] \tag{29}$$

From the inversion theorem, the surface temperature becomes

$$t_w^*(b,\ \infty,\ \tau)=\frac{Q_0a^2}{2\lambda t_0}ln\frac{b}{a}\equiv t_w^*(b,\ \infty,\ \infty) \tag{30}$$

Equation (30) indicates that λ can be determined from the constant value, t_w^* $(b,\ \infty,\ \infty)$, given by the equation. It is, however, an advantage of the hot wire method to determine λ before the surface temperature has a constant value, as mentioned above. So, Equation (30) is not used to determine λ in this study. To apply the hot wire method effectively, the measurement must be finished before the surface temperature reaches the steady constant value. From this point of view, it seems that there is a region of time needed effectively in the measurement. This region of time may be determined from the condition that the initial temperature wave caused by the heat from the wire exists far from the wire and further does not reach the outer wall of the material. In the region of time as above, $\sqrt{p}\ll 1$ and $\sqrt{p}\,b/a\gg 1$ are valid. Therefore, Equation (28) may be expanded in ascending powers of $\sqrt{p}$ and in descending powers of $\sqrt{p}\,b/a$ as follows;

$$\begin{aligned}T^*(b,\ \infty)=&-\frac{Q_0a^2}{2\lambda t_0}\frac{1}{p}\left[\frac{1}{2}ln\frac{C^2p}{4}+\frac{p}{4}\left\{-\frac{1-2A}{2}\left(ln\frac{C^2p}{4}\right)^2\right.\right.\\&\left.+(1-2B)ln\frac{C^2p}{4}-1\right\}+O(p^2)+\pi e^{-2(a/b)\sqrt{p}}\left(1\right.\\&\left.-\frac{1}{4}\frac{b}{a}\frac{1}{\sqrt{p}}+\frac{1}{32}\frac{a^2}{b^2}\frac{1}{p}\right)\left\{1+\frac{p}{2}\left[(1-2B)\right.\right.\\&\left.\left.\left.-(1-2A)ln\frac{C^2p}{4}\right]\right\}+O(p^2e^{-2(a/b)\sqrt{p}})\right]\end{aligned} \tag{31}$$

Using the inversion theorem, the surface temperature is obtained from Equation (31) as

$$\begin{aligned}t_w^*(b,\ \infty,\ \tau)=&\frac{Q_0a^2}{2\lambda t_0}\left[\frac{1}{2}ln\frac{4\tau}{c}+\frac{1}{4\tau}\left\{(1-2B)+(1-2A)ln\frac{4\tau}{c}\right\}\right.\\&+O\left(\frac{1}{\tau^2}\right)+\pi\left\{\mathrm{erfc}\,(\zeta)-\frac{1}{2}\left[\frac{1}{\sqrt{\pi}\zeta}e^{-2\zeta}-\mathrm{erfc}\,(\zeta)\right]\right.\\&\left.\left.+\frac{1}{32}\left[\left(\frac{1}{\zeta^2}+2\right)\mathrm{erfc}\,(\zeta)-\frac{2}{\sqrt{\pi}}\frac{1}{\zeta}e^{-\zeta^2}\right]\right\}+O\left(\frac{a^2}{b^2}\zeta e^{-\zeta^2}\right)\right]\end{aligned} \tag{32}$$

where $\zeta=b/(a\sqrt{\tau})$.

In the measurement, the radius of the thin wire is 1.5×10^{-2} cm, the radius of the material 0.75 to 5 cm and τ-value 20 to 1000. So, the terms, $O(1/\tau^2)$ and $O((a^2/b^2)\tau e^{-\zeta^2})$, are negligible in magnitude. To obtain λ from the slope of the plot t_w^* $(b,\ \infty,\ \tau)$ against $ln\ (\theta)$, the second and the fourth terms of the right side in Equation (32) must be negligible, compared to the first term. This condition may be satisfied within an error of 1 % if τ is determined from both Equation (25) and the relation

$$\zeta\geq 5 \quad \text{or} \quad b\geq 5\sqrt{\alpha\theta} \tag{33}$$

3) Semi-infinite Material ($b\to\infty$, $-l\leq z\leq l$)

Next, let us consider how long the material must be to obtain λ by the same procedure as that in an infinite material. In this case, Equation (17) becomes, taking account of $b\to\infty$,

$$T^*(b\to\infty,\ l<\infty)=\frac{Q_0a^2}{2\lambda t_0}\frac{1}{p}\sum_{n=0}^{\infty}\frac{4(-1)^n}{(2n+1)\pi}\mathrm{K}_0(\sigma_n)\Big/\Big[\Big\{\frac{\lambda_w}{2\lambda}\sigma_n^2+\Big(A-\frac{\lambda_w}{2\lambda}\Big)p\mathrm{K}_0(\sigma_n)+\Big\{1+\frac{\lambda_w}{2ah_{cr}}\sigma_n^2+\Big(B-\frac{\lambda_w}{2ah_{cr}}\Big)p\Big\}\sigma_n\mathrm{K}_1(\sigma_n)\Big] \tag{34}$$

Equation (34) is expanded in ascending powers of p and σ_n as follows, taking account of $p\ll 1$ and $\sigma_n\ll 1$;

$$T^*(\infty,\ l)=-\frac{Q_0a^2}{2\lambda t_0}\frac{1}{p}\sum_{n=0}^{\infty}\frac{4(-1)^n}{(2n+1)\pi}\Big[ln\frac{c\sigma_n}{2}+\sigma_n^2\Big\{\Big(\frac{1}{2}-\frac{\lambda_w}{2ah_{cr}}\Big)ln\frac{c\sigma_n}{2}+\Big(\frac{\lambda_w}{2\lambda}-\frac{1}{2}\Big)\Big(ln\frac{c\sigma_n}{2}\Big)^2-\frac{1}{4}\Big\}+p\Big\{\Big(A-\frac{\lambda_w}{2\lambda}\Big)\Big(ln\frac{c\sigma_n}{2}\Big)^2-\Big(B-\frac{\lambda_w}{2ah_{cr}}\Big)ln\frac{c\sigma_n}{2}\Big\}+\mathrm{O}(\sigma_n^4)\Big] \tag{35}$$

Using the inversion theorem again, we obtain the surface temperature of the form,

$$t_w^*(\infty,\ l,\ \tau)=-\frac{Q_0a^2}{2\lambda t_0}\sum_{n=0}^{\infty}\frac{4(-1)^n}{(2n+1)\pi}\Big[\frac{1}{2}\int_\tau^\infty(e^{-\Lambda_n\xi}/\xi)d\xi-(e^{-\Lambda_n\tau}/4\tau)\Big\{\Big(1+2B-\frac{2\lambda_w}{ah_{cr}}\Big)-(1-2A)ln\frac{4\tau}{C}+\mathrm{O}(\Lambda_n\int_0^\infty(e^{-\Lambda_n\xi}/\xi)d\xi)\Big] \tag{36}$$

where $\Lambda_n=\{(2n+1)\pi a/2l\}^2$ and ξ is an auxiliary variable.

In Equation (36), the term including Λ_0 has the greatest in magnitude, and the terms including Λ_1, Λ_2, ... become successively smaller and smaller exponentially in magnitude. So, only the value at $n=0$ of Equation (36) may be discussed to estimate the end effect. Moreover, $\Lambda_0\tau$ is small even though τ is large, because a/l is small. If $\Lambda_0\tau$ is small, the following relation can be used;

$$\int_\tau^\infty(e^{-\Lambda_0\xi}/\xi)d\xi=-C-ln\Lambda_0\tau+\Lambda_0\tau+\mathrm{O}\{(\Lambda_0\tau)^2\} \tag{37}$$

Then Equation (36) becomes

$$t_w^*(\infty,\ l,\ \tau)=\frac{Q_0a^2}{2\lambda t_0}\frac{2}{\pi}\Big[C+ln\Lambda_0\tau-\Lambda_0\tau+\mathrm{O}(\Lambda_0^2\tau^2)+\frac{e^{-\Lambda_0\tau}}{2\tau}\Big\{\Big(1+2B$$

$$-\frac{2\lambda_w}{ah_{cr}}\Big)+(1-2A)ln\frac{4\tau}{C}\Big\}+O(\Lambda_0 ln\Lambda_0\zeta)\Big] \tag{38}$$

In Equation (38), if the terms in the right side, $C+ln(\Lambda_0\tau)$, are remarkably larger than the other terms, λ may be determined by the slope of the plot t_w^* (∞, l, τ) against $ln(\theta)$. The fifth term including the thermal contact-resistance can be removed by taking account of the time lag in the same manner as that in an infinite material. Then, the right side in Equation (38) can be described by only the terms, $C+ln(\Lambda_0\tau)$, within an error of 1 %, if τ is determined by both Equation (25) and the relation

$$\Lambda_0\tau\lesssim 0.04 \quad \text{or} \quad l\gtrsim\left(\frac{\pi}{0.4}\right)\sqrt{\alpha\theta} \tag{39}$$

4) Finite Material ($a\leq r\leq b$, $-l\leq z\leq l$)

Let us discuss the radius and length of the material and the time for measurement required to obtain λ by the same procedure as that in an infinite material. The same procedure as that in an infinite material is valid if various factors are determined according to the following conditions;

a) the wire must be so small in radius and so good in thermal conductivity that the radial temperature profile in the wire becomes negligibly small compared to that in the material.

b) the radius of the material to be measured is determined by Equation (33).

c) the length of the material is determined by Equation (39).

d) the effective data needed to obtain λ must be chosen from the region of time which satisfies Equation (25). When we try to measure a thermal conductivity of a material, we often can estimate its rough value as a first step. Then the thermal diffusivity, α, can be estimated roughly. If the radius of the wire is given, the effective data needed to obtain λ must be chosen at a longer time than the elapsed time satisfied by Equation (25). Then, if the effective date were chosen in the region of time $\theta=\theta_1\sim\theta_2$ ($\theta_2>\theta_1$), θ_1, of course, must be larger than $20a^2/\alpha$, b must be larger than $5\sqrt{\alpha\theta_2}$, and l larger than $(\pi/0.4)\sqrt{\alpha\theta_2}$.

3. 1. 2. Experimental Apparatus and Procedure

Polyethylene sold at a shop was used as a standard sample, which was formed cylindrically, to demonstrate the validity of the above theory experimentally. The cylindrical sample was divided into two pieces along the axis. Along the axis of one of the two pieces, C-A thermocouples (0.3 mmϕ) enamelled for insulation and a constantan wire (0.3 mmϕ) used as a line heater were attached.

Fig. 3 shows a schematic diagram of the experimental apparatus. A polyethylene sample of a given radius and length (S) is maintained at a specified temperature level in a vessel (T_S). An electric current is passed through a thin constantan wire, using a storage battery (12 volts) (B). Magnitude of the electric current applied depends on the thermal conductivity of the material, to make the temperature rise a few degrees. In the present measurement, an electric current was passed through for about two minutes in the range of 0.4 to 0.8 amp., and a temperature rise in the wire was measured against an elapsed time for the two minutes. Using the data, a thermal conductivtiy λ was obtained by the following

equation, deduced from Equation (26) ;

$$\lambda=\frac{Q_0 a^2}{4(t_2-t_1)}\ ln\ \frac{\theta_2+\theta_0}{\theta_1+\theta_0} \qquad (26)'$$

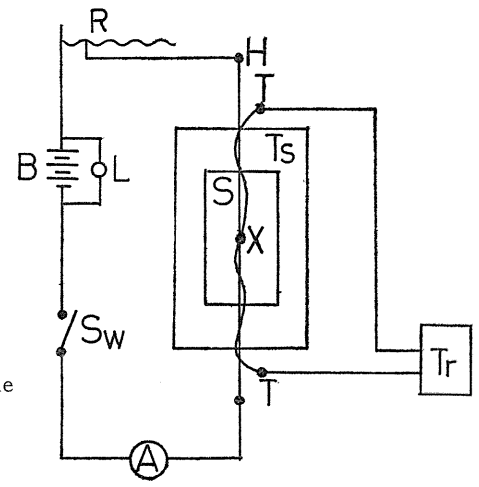

Fig. 3. A schematic diagram of the experimental apparatus.

3. 1. 3. Experimental Results and Discussion

The experimental results concerning the end effect are shown in Figs. 4 and 5. All of the data are chosen in the region of non-dimensional time, τ, of 100 to 1000. Fig. 4 shows that the radius of a polyethylene cylinder must be larger than 2.5 cm to avoid the end effect caused by the radius, while the length of polyethylene is

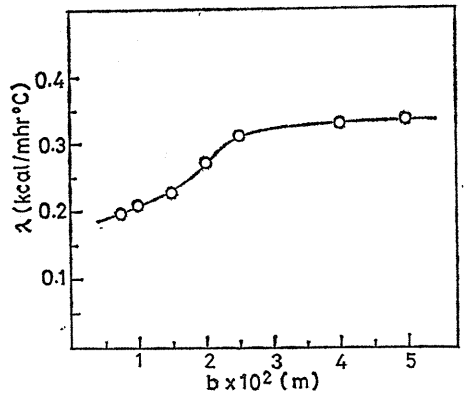

Fig. 4. An effect of the radius of material on the measurement of a thermal conductivity.

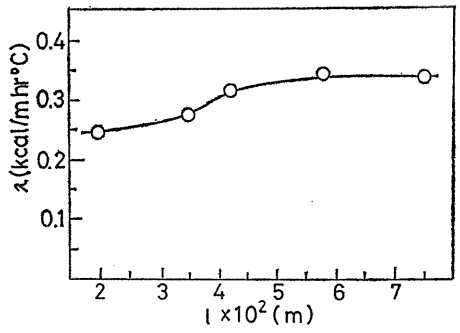

Fig. 5. An effect of the length of material on the measurement of a thermal conductivity.

fixed at 4 cm. Fig. 5 shows that the length of polyethylene must be greater than 4 cm to avoid the end effect caused by the length, while the radius is fixed at 2.5 cm. The critical values of the radius and the length may be determined theoretically by Equations (33) and (39) as follows;

$$b>5a\sqrt{\tau}=5\times 1.5\times 10^{-2}\times\sqrt{1000}=2.4cm$$

$$l>(\pi/0.4)a\sqrt{\tau}=(\pi/0.4)\times 1.5\times 10^{-2}\times\sqrt{1000}=3.7cm$$

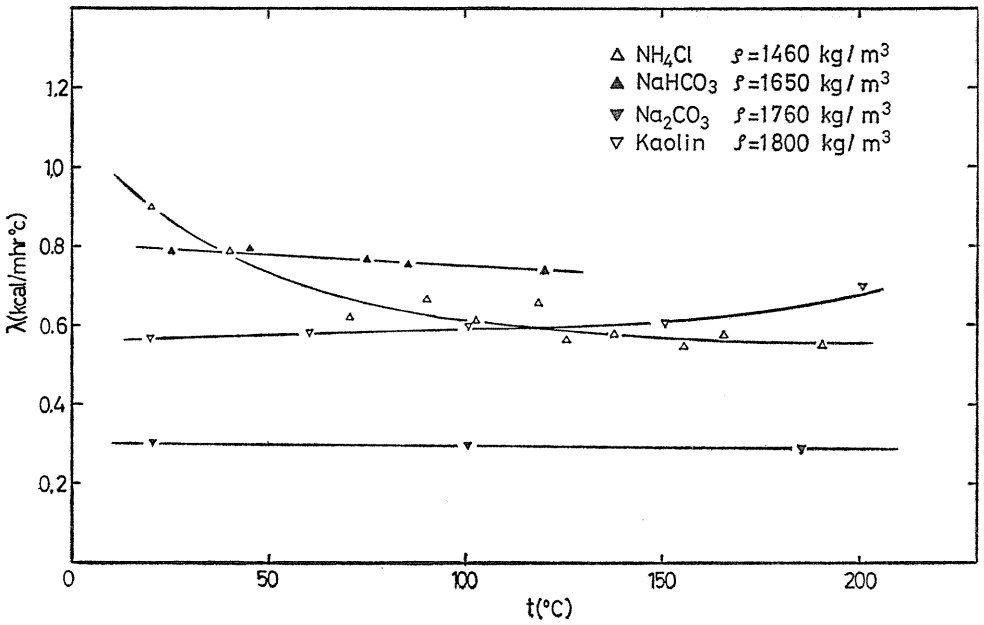

Fig. 6. Thermal conductivities in the non-reaction states measured by a hot wire method.

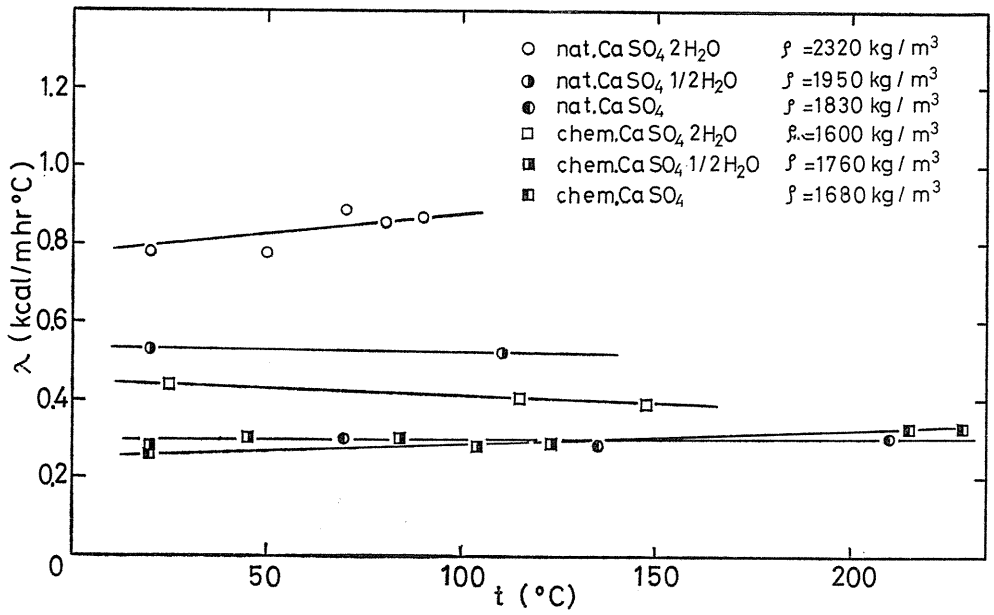

Fig. 7. Thermal conductivites in the non-reaction states measured by a hot wire method.

The theoretical estimation is in good agreement with the experimental results. From the above discussion, it was found that Equations (25), (33) and (39) might be applied to determine the critical dimensions of a material in measuring its thermal conductivity by the hot wire method. Avoiding the end effect according to the above theoretical considerations, the thermal conductivity measurements of the solid materials concerned in the present study by the hot wire method were carried out in the non-reaction states. Examples of the measured data are shown in Figs. 6 and 7.

3. 2. Measurement of Thermal Conductivity with Reaction[7, 8]

As is mentioned above, in the course of a solid reaction, in general, the rearrangement of the micro-crystal structure takes place. Therefore, it would be expected that the thermal conductivity during the period when the reaction (or the rearrangement of the crystal structure) is taking place has some different value from those in the non-reacting states (the pre- and the post-reaction states). This kind of the thermal conductivity (the thermal conductivity with reaction) is, in some cases, likely to be a more important basic property than those in the non-reacting states for discussing the relationships between the heat transfer and the overall rate of the reaction. Up to the present time, however, no effective measurements or no appropriate evaluation methods have been reported, the exception being the measurement by Mogilevsky & Chudnovsky.[9]

In this section, one of the effective methods of measuring the thermal conductivity with reaction is proposed, in which the principle of a D. T. A. (Differential Thermal Analysis) is applied in a suitable way. By the proposed method, the measurements are carried out for several kinds of crystal transformations and thermal decompositions which differ from each other in the reaction temperatures and in the heats of reaction. After eliminating effects of the changes in the macroscopic structural properties (like the void fraction) by the reaction, the measured thermal conductivities with reaction are compared with those in the non-reacting states. Effects of the reaction temperatures and the heats of reaction also are discussed.

3. 2. 1. Theory of Measurement

As has been mentioned in the foregoing section, thermal conductivities of solids are normally measured by the following two methods: a steady heat flow method and an unsteady heat flow method. Typical examples of these methods are: a cylindrical method and a twin-plate method for a steady heat flow method, and a hot-wire method for an unsteady heat flow one. These methods, in general, can be applied for measuring thermal conductivities of solids in the non-reacting states. However, it is difficult to measure the thermal conductivity with reaction by directly applying these methods, owing to the difficulties of eliminating the effects of unsteady heat absorption (or generation) accompanied by the reaction.

Thus, in the present study, the thermal conductivity with reaction was measured by applying the principle of a D. T. A. method. When the fundamental equations were derived for this method, the following assumptions were made:

(1) Both the reference sample (Ⅰ) and the reactant (Ⅱ) are cylindrical.

(2) The axial heat flow in the samples is negligible.

Based on the assumptions (1) and (2), the fundamental equations of unsteady heat conduction in each sample can be expressed as follows:

(Reference Sample)

$$c_{p\,\mathrm{I}}\rho_{\mathrm{I}}\left(\frac{\partial t_{\mathrm{I}}}{\partial\theta}\right)=\frac{1}{r}\frac{\partial}{\partial r}\left(\lambda r\frac{\partial t_{\mathrm{I}}}{\partial r}\right) \tag{40}$$

(Reactant)

$$c_{p\,\mathrm{II}}\rho_{\mathrm{II}}\left(\frac{\partial t_{\mathrm{II}}}{\partial\theta}\right)=\frac{1}{r}\frac{\partial}{\partial r}\left(\Lambda(t_{\mathrm{II}})r\frac{\partial t_{\mathrm{II}}}{\partial r}\right)-H\rho_{\mathrm{II}}\left(\frac{\partial k}{\partial\theta}\right) \tag{41}$$

where $\Lambda(t_{\mathrm{II}})$ denotes the thermal conductivity with reaction.

Setting the following variable:

$$\frac{\Lambda(t_{\mathrm{II}})}{\lambda}dt_{\mathrm{II}}=d\varphi \tag{42}$$

putting $c_{p\,\mathrm{I}}=c_{p\,\mathrm{II}}=c_p$ and $\rho=\rho_{\mathrm{I}}=\rho_{\mathrm{II}}$, and assuming c_p, ρ and λ to be constant during the measurement, we obtain Equation (43) by substracting Equation (40) from Equation (41).

$$\left(\frac{c_p\rho}{\lambda}\right)\frac{\partial T}{\partial\theta}+\frac{H\rho}{\lambda}\left(\frac{\partial k}{\partial\theta}\right)=\frac{1}{r}\frac{\partial}{\partial r}\left(r\frac{\partial(\varphi-t_{\mathrm{I}})}{\partial r}\right) \tag{43}$$

If we can assume that $\Lambda(t_{\mathrm{II}})/\lambda=1+K_2$, namely that the themal conductivity with reaction also is constant during the reaction, Equation (43) is rewritten as

$$\left(\frac{c_p\rho}{\lambda}\right)\frac{\partial T}{\partial\theta}+\frac{H\rho}{\lambda}\left(\frac{\partial k}{\partial\theta}\right)=\frac{1+K_2}{r}\frac{\partial}{\partial r}\left(r\frac{\partial T}{\partial r}\right)+\frac{K_2}{r}\frac{\partial}{\partial r}\left(r\frac{\partial t_{\mathrm{I}}}{\partial r}\right) \tag{44}$$

where T represents the differential temperature between the reactant and the reference sample, and is defined as $T=t_{\mathrm{II}}-t_{\mathrm{I}}$.

Integrating Equation (44), at first, with respect to time under the following initial and boundary conditions:

$$\left.\begin{aligned}&\theta=\theta_0,\ 0\leq r\leq a\ ;\ t_{\mathrm{I}}=t_{\mathrm{II}}=t_0\\&\theta=\theta_1,\ 0\leq r\leq a\ ;\ t_{\mathrm{I}}=t_{\mathrm{II}}=t_1\end{aligned}\right\} \tag{45}$$

$$\left.\begin{aligned}&\theta\geq\theta_0,\ r=a\ ;\ t_{\mathrm{I}}=t_{\mathrm{II}}=\gamma(\theta-\theta_0)+t_0\quad(\gamma\ ;\ a\ \text{constant})\\&\qquad r=0\ ;\ \partial t_{\mathrm{I}}/\partial r=\partial t_{\mathrm{II}}/\partial r=0\end{aligned}\right\} \tag{46}$$

where the subscripts 0 and 1 express the initial and the final stages of the reaction respectively, we get

$$\frac{Q}{\lambda}=\frac{1+K_2}{r}\frac{\partial}{\partial r}\left[r\partial\left(\int_{\theta_0}^{\theta_1}Td\theta\right)\Big/\partial r\right]+\frac{K_2}{r}\frac{\partial}{\partial r}\left[r\partial\left(\int_{\theta_0}^{\theta_1}t_{\mathrm{I}}d\theta\right)\Big/\partial r\right] \tag{47}$$

where Q $(=H\rho)$ denotes the heat of reaction per unit volume. Again, integrating Equation (47) with respect to r, we obtain

$$\int_0^a\frac{Q}{2\lambda}rdr=-(1+K_2)\int_{\theta_0}^{\theta_1}T_c d\theta+K_2\int_{\theta_0}^{\theta_1}(t_{\mathrm{I},\,s}-t_{\mathrm{I},\,c})d\theta \tag{48}$$

where T_c means the differential temperature at the center, or the D. T. A. peak.

Introducing $t_{I,s}-t_{I,c}\doteqdot\Delta t_{I\,av}$ into the second term of the right-hand side of Equation (48), we finally obtain

$$K_2=\frac{\Lambda-\lambda}{\lambda}=\left[\frac{Qa^2}{4\lambda}+\int_{\theta_0}^{\theta_1}T_c d\theta\right]\Big/\left[-\int_{\theta_0}^{\theta_1}T_c d\theta+\Delta t_{I\,av}(\theta_1-\theta_0)\right] \qquad (49)$$

Thus, by measuring the peak area of the D. T. A. curve and the average temperature difference between the surface and the center of the reference sample, the thermal conductivity with reaction can be determined by Equation (49).

3. 2. 2. Experimental Apparatus and Procedure

1) Samples

As is mentioned above, several kinds of crystal transforming and thermally decomposing solid reactants were employed as samples for the present measurements.

Those are: ammonium chloride, silver iodide, quartz and barium carbonate for crystal transformation, and sodium bicarbonate, gypsum (natural- and chemical-), calcium hydroxide and marble for thermal decomposition. Natural gypsum was from Africa with a purity of more than 98 %, and marble (white) from Greece, whose purity more than 98 %. The other samples were powdered, of reagent grade with a purity more than 99 %. Each powdered sample was formed into a cylindrical shape (8.0 mm diameter and 18.0 mm length) by pressing. A chromel-alumel thermocouple wire (0.3 mmϕ) was inserted along the axis through a small hole drilled to measure the temperature at the center of each sample. Natural gypsum and marble also were formed into the same shape by cutting and shaving, and a small hole was drilled similarly. Before the measurement, the samples were well dried in a desiccator.

The physical properties and the type of reaction of each sample are presented in Table 1. As is seen from the table, those samples are much different from each other in the reaction temperatures and the heats of reaction. Therefore, it seems possible to relate the expected differences among the measured data to the reaction temperatures or the heats of reaction and to discuss the theoretical background of the thermal conductivity with reaction.

It is necessary that the reference sample does not react in the range of the reaction temperature of the reactant and that it has, as closely as possible, a similar value of the thermal diffusivity to that of the reactant. In this measurement, sodium carbonate was chosen as the reference sample for sodium bicarbonate, and anhydride gypsum for gypsum, and calcium oxide both for calcium hydroxide and for marble. For the crystal transformation, three to five kinds of materials: kaolin, sodium carbonate, natural anhydride gypsum, silica and calcium oxide were used, and the results were compared between these samples. The physical properties of the reference samples used are presented in Table 1, together with those of the reactants. The values of the heats of reaction and the specific heats were obtained from the Chemistry Handbook, Japan, and those of the thermal conductivities in the non-reaction states were measured by the hot-wire method, discussed previously. Since the densities of the samples (void fractions) scattered slightly (except for the natural gypsum and the marble) owing to slight variations of the conditions of pressing, the effects of these variations on the λ-values were corrected by the Kunii-Smith's equation[10], and the corrected values were applied to Equation (49).

Table 1. Physical properties of the samples employed.

Sample	H (kcal/kg)	c_p (t) (kcal/kg℃)	ρ (ε) (kg/m³)	λ (t) (kcal/m hr ℃)	Reaction Temp. (℃)	Type of Reaction
$NaHCO_3$	204.3	0.289(120℃)	1650(0.25)	0.73(120℃)	125～135	dehydration and decarbonization
n. $CaSO_4 \cdot 2H_2O$	116.9	0.285(130℃)	2320(0.0)	0.90(120℃)	130～140	dehydration
n. $CaSO_4 \cdot 1/2H_2O$	27.6	0.258(190℃)	1951(0.26)	0.52(160℃)	190～200	dehydration
c. $CaSO_4 \cdot 2H_2O$	116.9	0.283(115℃)	1601(0.31)	0.37(110℃)	120～130	dehydration
c. $CaSO_4 \cdot 1/2H_2O$	27.6	0.258(190℃)	1762(0.33)	0.28(190℃)	190～200	dehydration
$Ca(OH)_2$	337.0	0.361(500℃)	1650(0.26)	1.85(500℃)	520～540	dehydration
$CaCO_3$	426.0	0.307(900℃)	2710(0.0)	2.30(900℃)	900～920	decarbonization
NH_4Cl	18.7	0.495(180℃)	1460(0.05)	0.55(180℃)	184～189	CsCl⇄NaCl
AgI	6.3	0.066(127℃)	5030(0.14)	0.16(145℃)	147～152	$\alpha \rightleftarrows \beta$
SiO_2	2.5	0.295(570℃)	1954(0.26)	0.53(570℃)	573～578	$\alpha \rightleftarrows \beta$
$BaCO_3$	18.0	0.167(670℃)	3607(0.19)	1.18(800℃)	810～820	$\beta \rightleftarrows \gamma$
Na_2CO_3		0.288(150℃)	1756(0.31)	0.29(150℃)		
Kaolin		0.198(180℃)	1802(0.31)	0.65(180℃)		
n. $CaSO_4$		0.200(190℃)	1830(0.38)	0.30(200℃)		
c. $CaSO_4$		0.200(190℃)	1681(0.43)	0.32(200℃)		
CaO		0.220(500℃)	1340(0.60)	1.00(600℃)		

2) Heating Apparatus

A sketch of the heating apparatus employed is shown in Fig. 8. As shown in Fig. 8, the apparatus consisted of an iron tube (100 mm, I. D. and 500 mm, height), three pieces of 1 kW kanthal wire wound separately around the tube, and refractory and insulating bricks. The temperature of the tube wall was measured with 0.3 mmϕ chromel-alumel thermocouples at three points, and recorded continuously by an automatic temperature recorder. After the sample holder was set in the middle part of the tube, where the temperature was kept uniform, the holder was heated at a certain constant rate by adjusting the voltage of the slide transformer connected with each wire.

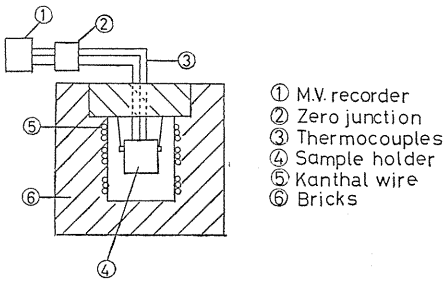

Fig. 8. A schematic drawing of the heating apparatus.

3) Sample Holder

The details of the sample holder are shown in Fig. 9. The sample holder was made of a cylindrical steel block, 60 mm diameter and 90 mm height. As illustrated in Fig. 9, two holes of 8.0 mm diameter and 30 mm height were drilled in a symmetrical position from the center axis of the holder to hold the reactant and the

reference sample, respectively. The temperature of the holder was measured with a 0.3 mmϕ chromel-alumel thermocouple inserted along the center axis of the holder.

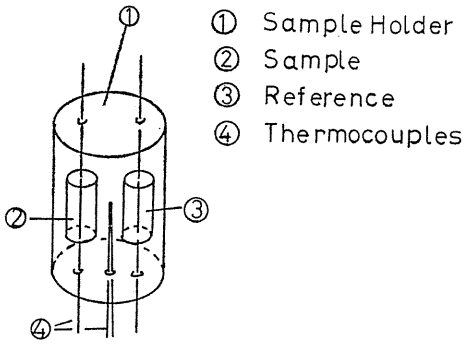

Fig. 9. Details of the sample holder.

4) Experimental Procedure

After chromel-alumel thermocouples (0.3 mmϕ) were inserted into the reactant, the reference sample and the sample holder as shown in Fig. 9, each thermocouple was connected with a mV-recorder and an automatic temperature recorder. Then, the sample holder was placed in the proper position in the heating tube, and the heating was started. The temperature of the tube wall was carefully controlled so that the sample holder would be heated at a constant rate, and the differential temperature between the reactant and the reference sample was recorded continuously by a mV-recorder. As for the ammonium chloride, after the heating experiment was completed, the sample holder was cooled at a constant rate from near 200 ℃, and the differential temperature was again measured (cooling experiment). At the same time, the average temperature difference, $\Delta t_{I\,av}$ was measured with another differential thermocouple. In Equation (49), however, the values of $\Delta t_{I\,av}(\theta_1-\theta_0)$ were lower than 5 % of the peak area of D. T. A. curves, and their contributions were relatively small.

3. 2. 3. Results and Discussion

Examples of the D. T. A. curves obtained from the measurements are shown in Figs. 10 to 12. As described previously, the thermal conductivity with reaction, A, can be calculated from the peak area of the D. T. A. curve by Equation (49). These calculated values of A are tabulated in Tables 2 to 11.

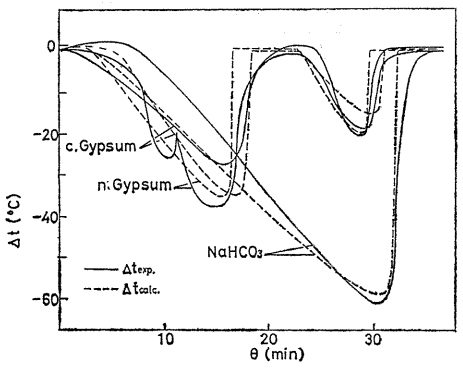

Fig. 10. D. T. A. curves of sodium bicarbonate and gypsum (natural- and chemical-).

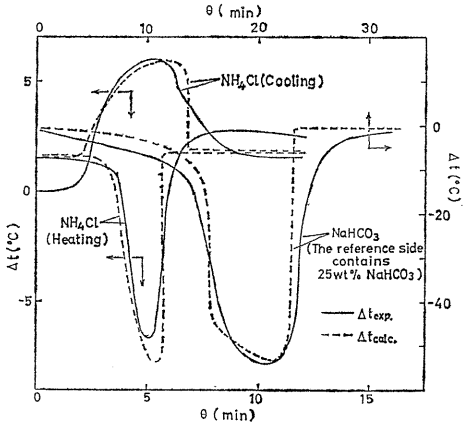

Fig. 11. D. T. A. curves of sodium bicarbonate and ammonium chloride (heating and cooling).

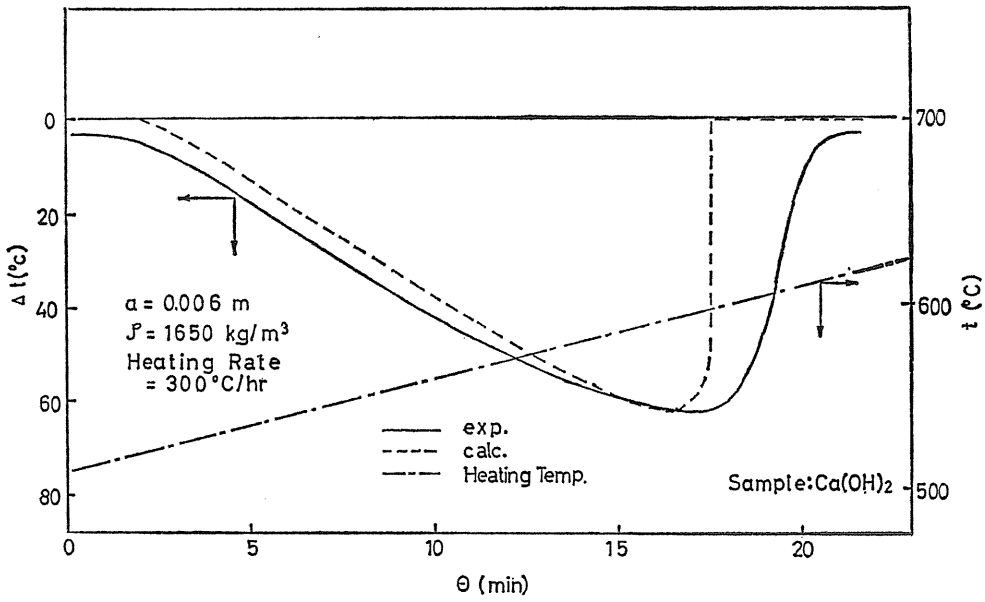

Fig. 12. A D. T. A. curve of calcium hydroxide.

Table 2. Dehydration and decarbonization of $NaHCO_3$.

No.	$dt/d\theta$	ε	λ	Λ_i	Λ_m	Λ_f	Λ_s	λ_s	λ'
1.	170	0.04	0.90	0.20	0.20	0.17	0.31	3.60	0.33
2.	400	0.05	0.89	0.23	0.23	0.20	0.38	3.60	0.33
3.	580	0.14	0.81	0.20	0.15	0.16	0.36	3.60	0.30

Table 3. Dehydration of natural $CaSO_4 \cdot 2H_2O$.

No.	$dt/d\theta$	ε	λ	Λ_i	Λ_m	Λ_f	Λ_s	λ_s	λ'
6.	25	0.0	0.90	0.26	0.24	0.21	0.29	0.90	0.52
7.	110	0.0	0.90	0.28	0.27	0.25	0.32	0.90	0.52
8.	190	0.0	0.90	0.25	0.24	0.22	0.29	0.90	0.52

Table 3′. Dehydration of natural $CaSO_4 \cdot 1/2H_2O$.

No.	$dt/d\theta$	ε	λ	Λ_i	Λ_m	Λ_f	Λ_s	λ_s	λ'
6.	25	0.26	0.52	0.25	0.22	0.19	0.45	0.70	0.30
7.	110	0.26	0.52	0.23	0.22	0.21	0.42	0.70	0.30
8.	190	0.26	0.52	0.19	0.17	0.17	0.34	0.70	0.30

Table 4. Dehydration of chemical $CaSO_4 \cdot 2H_2O$.

No.	$dt/d\theta$	ε	λ	Λ_i	Λ_m	Λ_f	Λ_s	λ_s	λ'
4.	250	0.17	0.61	0.19	0.18	0.17	0.29	1.95	0.40
5.	240	0.15	0.63	0.22	0.21	0.19	0.34	1.95	0.41

Table 4'. Dehydration of chemical $CaSO_4 \cdot 1/2H_2O$.

No.	$dt/d\theta$	ε	λ	Λ_i	Λ_m	Λ_f	Λ_s	λ_s	λ'
4.	250	0.43	0.40	0.15	0.14	0.13	0.29	1.10	0.32
5.	240	0.40	0.41	0.16	0.15	0.14	0.25	1.10	0.32

Table 5. Crystal transformation of NH_4Cl (heating).

No.	$dt/d\theta$	ε	λ	Λ	Λ_s	λ_s	λ'
9.	85	0.04	0.57	0.46	0.77	1.10	0.57
10.	140	0.02	0.58	0.46	0.76	1.10	0.58

Table 6. Crystal transformation of NH_4Cl (cooling).

No.	$dt/d\theta$	ε	λ	Λ	Λ_s	λ_s	λ'
9.	−60	0.04	0.57	0.45	0.77	1.10	0.57
10.	−175	0.02	0.58	0.45	0.74	1.10	0.58

Table 7. Crystal transformation of AgI.

No.	$dt/d\theta$	ε	λ	Λ	Λ/λ	λ'
22.	25	0.14	0.16	0.11	0.72	0.16
23.	100	0.14	0.16	0.12	0.77	0.16
24.	−30	0.14	0.16	0.11	0.72	0.16

Table 8. Crystal transformation of SiO_2.

No.	$dt/d\theta$	ε	λ	Λ	Λ/λ	Λ_s/λ_s
11.	190	0.26	0.53	0.54	1.03	1.01
12.	320	0.25	0.54	0.53	0.99	0.99
13.	−210	0.26	0.53	0.52	0.98	0.98

Table 9. Crystal transformation of $BaCO_3$.

No.	$dt/d\theta$	ε	λ	Λ	Λ/λ	Λ_s/λ_s
14.	155	0.19	1.18	0.54	0.46	0.46
15.	205	0.19	1.18	0.43	0.36	0.36
16.	−140	0.19	1.18	0.49	0.42	0.42

Table 10. Dehydration of $Ca(OH)_2$.

No.	$dt/d\theta$	ε	λ	Λ	Λ/λ	λ'
20.	175	0.26	1.85	0.44	0.24	1.00
21.	300	0.26	1.85	0.46	0.25	1.00

Table 11. Decarbonization of $CaCO_3$.

No.	$dt/d\theta$	ε	λ	Λ	Λ/λ	Λ_s/λ_s
17.	75	0.0	2.30	0.64	0.28	0.38
18.	110	0.0	2.30	0.69	0.30	0.41
19.	175	0.0	2.30	0.68	0.29	0.41

In the calculation of the peak area, the base line was determined by the method of Rose, et al.[11], and the curve was integrated graphically. In Tables 2 to 11 λ and Λ denote the effective thermal conductivity in the pre-reaction state and that with reaction, respectively. Also, λ_s and Λ_s are: the thermal conductivity of the crystal in the pre-reaction state and that with reaction, respectively. The thermal conductivities of the crystals shown in the tables are the values calculated back from the effective thermal conductivities by the Kunii-Smith's equation[10] in the case of the powder sample, or by the Kingery's equation[12] in the case of both natural gypsum and marble. For the calculation of Λ by Equation (49), the value of the thermal conductivity in the non-reaction state (the λ-value) is required. In the progress of a solid reaction such as thermal decomposition, however, the λ-value itself is considered to vary owing to the change of the void fraction and the crystal structure.

In the present study, therefore, three kinds of λ-values: λ, λ' (the thermal conductivity in the post-reaction state) and the arithmetical mean of λ and λ': were applied to the calculation of the Λ-value in the case of thermal decomposition and the calculated results were compared with one another. In Tables 2 to 4', these three kinds of Λ-values are denoted by Λ_i, Λ_f and Λ_m respectively. It is seen that Λ_i Λ_m and Λ_f are observed to be in a fairly good agreement. Thus, hereafter the discussion will be presented on the basis of the Λ_i-values, and on the basis of the Λ_s-values which were calculated from the Λ_i-values.

The following interesting results can be deduced from Tables 2 to 11: the effective thermal conductivity with reaction, Λ, is smaller than both the effective thermal conductivity in the pre-reaction state, λ, and that in the post-reaction state, λ', and the Λ-value obtained for each reactant is almost constant inde-

pendently of the heating rate. It was also confirmed for the crystal transformations employed that the reference samples have little, if any, effects on the measurements and that the Λ-value for each reactant is almost independent of any reference samples employed in the present measurements. This was tested mainly using the ammonium chloride. As is seen from Tables 5 and 6, in both the heating and the cooling experiments of the ammonium chloride, the Λ-values obtained also were almost the same. In addition, for the marble which reacts at the highest temperature among the reactants employed, an effect of the diameter of the sample was tested in the range of 9 to 14 mm. However, no appreciable effect was observed.

When thermal decomposition takes place, a diffusion rate of the decomposed gas or liquid sometimes produces some effects on the reaction. For this reason, the application of Equation (49) to thermal decomposition would be questionable under some experimental conditions where the diffusion rate has a larger effect. However, as pointed out previously and as demonstrated later, the effect of the diffusion rate is usually much smaller than that of the heat transfer rate in the case of the sample reactant employed.

Therefore, it can be concluded that the thermal conductivity with reaction has truely a considerably smaller value than that in the non-reaction state, although the absolute value of Λ itself contains an uncertainty in the case of thermal decomposition. In Fig. 13, the average value of the ratio, Λ to λ, (or Λ_s to λ_s) obtained for each reactant is plotted against the heat of its reaction per unit volume, Q. In a preliminary discussion, we have tested a few kinds of plots concerning the relations between the ratio, Λ to λ, and the parameters expected to be related. However, the parameters other than the heat of reaction have been observed to have no methodical relations to the ratio, Λ to λ. Even the reaction temperature and the type of reaction are unlikely to be related reasonably to the ratio. Therefore, it has been concluded that only the heat of reaction is the parameter to have a methodical relation to the ratio.

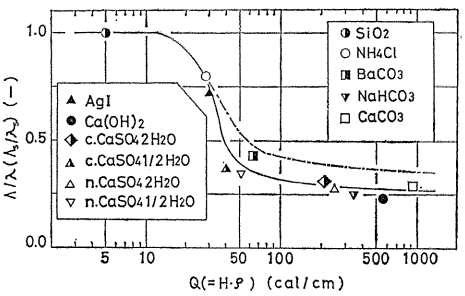

Fig. 13. The relation Λ/λ and the heat of reaction.

It is seen from Fig. 13 that the ratio, Λ/λ, decreases with increase in the Q-value in a similar form to that of a probability distribution function. The curve starts from about unity for the quartz, which has the smallest heat of reaction among the reactants employed, and reaches around 0.25 for the marble with the largest heat of reaction. Hereafter, the curve seems to be saturated.

In an endothermic solid reaction like crystal transformation and thermal decomposition, the heat of reaction generally can be roughly related to the activation energy of its reaction. As is well known, the activation energy of such reaction is a good measure of disorder or disintegration of the crystal lattice which would take place during the very period when the reaction takes place.

The theoretical background of the reason why the value of Λ (or Λ_s) is smaller

than those of λ and λ' (or λ_s) would be very complicated. However, it is suggested from the results and the discussion through Fig. 13, as one of the principal reasons, that the crystal lattice assumes a disordered or disintegrated state (the pseudo-amorphous state) owing to the violent thermal vibration of the bonded molecules, and that the dependency of the ratio, A to λ, (or A_s to λ_s) on the Q-value represents the change in a degree of disorder or disintegration. In the low and the medium temperature range, the thermal conductivity of an amorphous solid is usually smaller than that of a crystal. In a similar temperature range, the specific heat of an amorphous solid is nearly the same as that of a crystal, or is slightly smaller. Therefore, it seems reasonable that the specific heat is assumed constant in comparison with the heat of reaction.

As has been discussed in the theory of measurement, in the present method, the thermal conductivity with reaction was determined only on the basis of the peak area of the D. T. A. curve (the basic equation was first integrated with respect to time). Also, in the case of thermal decomposition, the diffusion rate of the decomposed gas may have some effects on the determination. Therefore, it seems advisable to confirm theoretically the reappearance of the peak shape and the peak temperature of the D. T. A. curve.

If the concept of the overall specific heat described in Section 2. is valid, and if the type (a) or the type (c) shown in Fig. 1 is assumed to the relation between the overall specific heat and the temperature, Equation (44) is rewritten as

$$\left(\frac{c_p\rho}{\lambda}\right)\left(\frac{\partial T}{\partial\theta}\right)+\left(\frac{c_p\rho K_1}{\lambda}\right)\left(\frac{\partial t_{\mathrm{II}}}{\partial\theta}\right)=\left(\frac{1+K_2}{r}\right)\frac{\partial}{\partial r}\left(r\frac{\partial T}{\partial r}\right)+\frac{K_2}{r}\frac{\partial}{\partial r}\left(r\frac{\partial t_{\mathrm{I}}}{\partial r}\right) \quad (50)$$

where $K_1=H/\{c_p(t_{\mathrm{II}f}-t_{\mathrm{II}i})\}$. $t_{\mathrm{II}i}$ and $t_{\mathrm{II}f}$ denote the initial and the final temperatures of the reaction. Equation (50) with the initial and the boundary conditions, Equations (45) and (46), was solved by a numerical method using the thermal conductivities with reaction which were obtained in these measurements, and a comparison was made between the theoretical D. T. A. curve and the experimental one. Examples of the results are shown in Figs. 10 to 12.

Furthermore, taking sodium bicarbonate as an example, a comparison was made for the case that some quantity of sodium bicarbonate was added to the reference sample, and this example is shown in Fig. 11. Through Figs. 10 to 12, it is observed that the theoretical and the experimental D. T. A. curves are in a fairly good agreement with regard to the peak shape, the peak temperature and the peak time.

Summarizing the above results, it was shown that the thermal conductivity with reaction was smaller than those in both the pre- and the post-reaction states. Furthermore, it was also noted that the crystal thermal conductivity with reaction, which was excluded from the effects of the void fraction, became almost constant for every reactant, independently of the experimental conditions, and that temporary disorder or disintegration of the crystal lattice during the very period of the reaction was assumed to cause such differences between the thermal conductivity with reaction and those in the non-reacting states.

4. Unsteady Heat Conduction Accompanied by an One-Stage Endothermic Solid Reaction

In this section, an unsteady heat conduction problem accompanied by an one-stage endothermic solid reaction is dealt with theoretically. The term, 'One-Stage', means that the reaction concerned takes place singulary under the condition given, only in the one-narrow and limited temperature range. We have a number of examples of this type of endothermic solid reactions. Those are: the crystal transformations of ammonium chloride, silver iodide, quartz, barium carbonate and others, and the thermal decompositions of sodium bicarbonate, kaolinite, calcium hydroxide, calcium carbonate and others.

As is seen from the foregoing discussions, the principal interests of the present theoretical analysis are in the overall specific heat and in the thermal conductivity with reaction. The applicabilities of the overall specific heat to those one-stage reactions have already been discussed partially in the author's previous works concerning the cyrstal transformations of ammonium chloride, quartz and barium carbonate[13] and the thermal decompositions of sodium bicarbonate[14] and kaolinite[15]. In this section, therefore, it is intended to discuss an effect of the thermal conductivity with reaction on the unsteady heat conduction accompanied by the one-stage endothermic reaction as well as the applicability of the overall specific heat.

The theoretical results obtained from a numerical treatment of the basic differential equations are compared with the experimental data measured in the experiment of one-dimensional, unsteady heat conduction in both a sphere and a slab. The reactants chosen for the experiment are calcium hydroxide and calcium carbonate, which have recently an increasing new need in the area of the recovery or the storage of waste heats. The theoretical results also are compared with the results calculated from the theory which does not involve an effect of the thermal conductivity with reaction.

4. 1. Theoretical Analysis

The basic equations for one dimensional, unsteady heat conduction accompanied an endothermic solid reaction can be written as follows, using the concept of overall specific heat:

(For a sphere)

$$C_p(t)\rho\left(\frac{\partial t}{\partial \theta}\right)=\frac{1}{r^2}\frac{\partial}{\partial r}\left(\lambda(t)r^2\frac{\partial t}{\partial r}\right) \tag{51}$$

(For a slab)

$$C_p(t)\rho\left(\frac{\partial t}{\partial \theta}\right)=\frac{\partial}{\partial x}\left(\lambda(t)\frac{\partial t}{\partial x}\right) \tag{52}$$

where $\lambda(t)$ is a thermal conductivity of a solid and has a different value, the thermal conductivity with reaction, in the range of the reaction temperature, from those in the non-reaction states. The initial and the boundary conditions of Equations (51) and (52) are:

(For a sphere)

$$\left.\begin{aligned} &\theta=0, \quad 0\leq r\leq a\,; \quad t=t_0 \\ &\theta\geq 0, \quad r=a\,; \quad \left(\frac{\partial t}{\partial r}\right)=\left(\frac{h}{\lambda}\right)(t_w-t_s) \\ &\qquad\quad r=0\,; \quad \left(\frac{\partial t}{\partial r}\right)=0 \end{aligned}\right\} \tag{53}$$

(For a slab)

$$\left.\begin{aligned} &\theta=0, \quad 0\leq x\leq L\,; \quad t=t_0 \\ &\theta\geq 0, \quad x=L\,; \quad \left(\frac{\partial t}{\partial x}\right)=\left(\frac{h}{\lambda}\right)(t_w-t_s) \\ &\qquad\quad x=0\,; \quad \left(\frac{\partial t}{\partial x}\right)=0 \end{aligned}\right\} \tag{54}$$

where t_0, t_w and t_s denote a certain constant temperature below the reaction temperature, a heating temperature and the surface temperature of a sample, respectively, and L is the thickness of a slab.

As has already been discussed in Section 2., if the concept of the overall specific heat is valid for the reaction concerned, the fraction of the reaction (the conversion) can be dealt with as a function of temperature only. Therefore, at the same time, it is also allowed to deal with the physical properties of the solid as a function of temperature. This is illustrated schematically in Fig. 14. Since, in Fig. 14, it is assumed that the conversion increases linearly with increase in temperature after the reaction starts, both the values of $C_p(t)$ and $\lambda(t)$ also become constant in the range of the reaction temperature. Although such a linear relation between the conversion and the reaction temperature is not necessarily true (therefore, both $C_p(t)$ and $\lambda(t)$ also do not have the constant values.), this assumption may be useful to reduce the troubles in a calculational procedure.

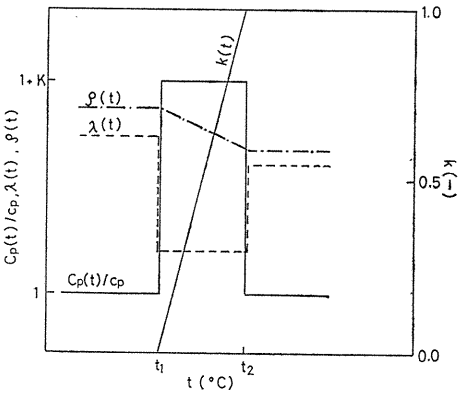

Fig. 14. Illustrative variations of the physical properties of a sample.

Dividing a sphere (or a slab) into a thin shell (or a thin sheet) with a constant space interval, s, in the direction of heat flow and rewriting Equation (51) (or Equation (52)) into the form of a difference equation, we get, for the i-th increment (except for the first and the final increments),

$$\Delta t_i=\frac{1}{C_p(t_i)\rho(t_i)V_i}\left[A_{i+\frac{1}{2}}\left\{\frac{\lambda(t_{i+1})+\lambda(t_i)}{2}\right\}\frac{t_{i+1}-t_i}{s}\right.$$

$$-A_{i-\frac{1}{2}}\left\{\frac{\lambda(t_i)+\lambda(t_{i-1})}{2}\right\}\left[\frac{t_i-t_{i-1}}{s}\right]\Delta\theta \tag{55}$$

where Δt_i denote a temprature increase during a time interval, $\Delta\theta$, and A and V are a heat conduction area (a geometric mean area beween the two increments) and a volume of the increment, respectively. Calculating Equation (55) numerically according to a successive method, we can obtain a theoretical, unsteady temperature distribution in a sphere (or in a slab).

The theoretical results thus obtained by assuming the physical properties illustrated schematically in Fig. 14 is denoted, hereafter, by 'calc. 1', and the results calculated from the theory which assumes constant physical properties, by 'calc. 2'. In the 'calc. 2', only the overall specific heat is assumed to be the same as that in the 'calc. 1', and the other properties, those in the post-reaction state.

As is described later, in the present experiment, a coupled radiation and natural convection heat transfer concerns the boundary condition on the surface of the sample. Therefore, a heat transfer coefficient, h, is expressed in both the theories as follows:

$$h=h_c+h_r \tag{56}$$

$$\left.\begin{aligned} h_c&=\alpha(t_w-t_s)^{1/4}\\ h_r&=\phi_{s-w}\sigma(T_w+T_s)(T_w^2+T_s^2)\end{aligned}\right\} \tag{57}$$

where h_c and h_r denote a natural convection- and a radiation-heat transfer coefficient, respectively, and ϕ_{s-w}, σ and T, an overall gray absorptivity of radiation, a Stefan-Boltzmann constant and absolute temperature, respectively.

4. 2. *Experimental Apparatus and Procedure*

4. 2. 1. *Samples*

A solid sphere and a solid slab employed in the present experiment were formed by pressing powdered calcium hydroxide of reagent grade. The diameters of spherical samples were 1.0, 2.0, 3.0 and 4.0 cm, and the thickness of a slab sample (a disc of 18 cm in diameter), was in the range of 2.0 to 5.0 cm. A special care was taken of pressing the powdered sample to depress a scatter in the values of the density and the thermal conductivity of the solid sample formed. Thus, the densities of the solid samples were: 1660±10 kg/m^3 for the spherical sample, and 1430±20 kg/m^3 for the slab sample, respectively.

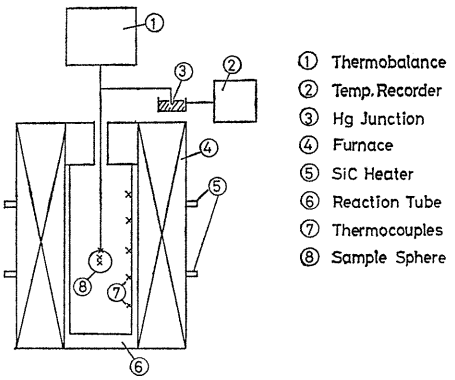

Fig. 15. (a) An experimental apparatus used for a spherical sample.

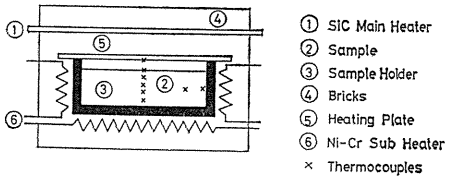

Fig. 15. (b) An experimental apparatus used for a slab sample.

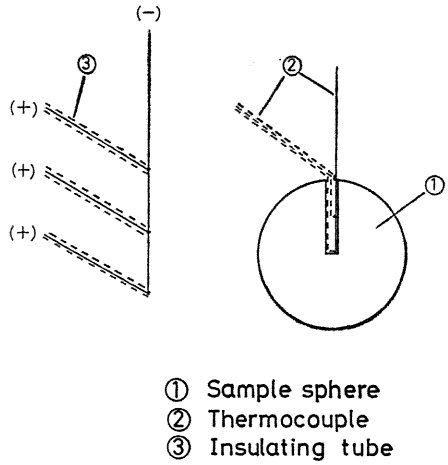

Fig. 15. (c) Details of the thermocouple connection employed for temperature measurement in a spherical sample.

4. 2. 2. Heating Apparatus

1) For a Spherical Sample

A schematic drawing of the heating apparatus used for a spherical sample is shown in Fig. 15 (a). A porcelain reaction tube of 9.0 cm in inner diameter and 60.0 cm in height was heated from the surroundings in a vertical electric furnace with eight rod heaters made of silicon carbide. Above the top of the furnace, a thermo-balance of a minimum sensitivity of 0.1 mg was mounted to measure a weight decrease in the sample with the reaction. The temperature on the whole inner surface of the reaction tube (the heating temperature) was kept at a given constant in the range of 650 to 750 ℃ by controlling an electric current passing through the rod heaters by seperate four slide-transformers. After a sample sphere was placed at a fixed position in the reaction tube, the measurement of unsteady temperature distribution and weight decrease in the sphere placed was started. The temperature distribution was measured with chromel-alumel thermocouples and recorded continuously on an automatic temperature recorder. The weight decrease was measured at a time interval of one to two minutes. To enable the simultaneous measurement of temperature and weight, the thermocouple wires were connected with the lead wires of the temperature recorder through a liquid mercury pool (a Hg-junction).

2) For a Slab Sample

A porcelain tube of 22.5 cm in diameter and 7.0 cm in height was used as the reaction tube for a slab sample. The above mentioned slab sample (the disc) was set in the tube as illustrated in Fig. 15 (b), and the powdered sample was filled up in the gap between the side wall of the sample and the inner wall of the tube. A stainless steel plate of 5 mm in thickness (a heating plate) was placed on the top of the reaction tube and heated uniformly from above by eight rod heaters of silicon carbide, which were arranged across each other. The heating temperature

(the temperature on the lower surface of the plate) was raised exponentially with time in the form, $t_w=t_0+t_H\{1-\exp(-\beta\theta)\}$. To satisfy the boundary condition on the lower surface of the sample, $x=0$; $(\partial t/\partial x)=0$ (adiabatic), the lower surface also was heated by a nichrome wire heater of 2 kw-power through an insulating brick disc, and the adiabatic condition was monitored by measuring the temperature distribution in the brick disc. On the outer side wall of the reaction tube, another auxiliary nichrome wire heater was wound to make the heat loss from the side wall the minimum with aid of an insulator. The heat loss also was monitored by measuring the radial temperature distribution in the sample disc.

4. 2. 3. Measurement of Temperature Distribution

Fig. 15 (c) shows the details of the thermocouple connection used to measure the unsteady temperature distribution in the spherical sample. The shrinkage of a solid sample usually takes place with dehydration of calcium hydroxide. Therefore, it is necessary for measuring the temperature distribution accurately to hold the thermocouple bead at a fixed position in the sample with a special care. For this sake, in making the connections of thermocouples for the spherical sample, the wire of negative side was shared with the wires of positive side as shown in Fig. 15 (c). Thus, the interval between the temperature measurement positions was kept constant throughout, even though the shrinkage took place. In the case that the shrinkage is relatively small, other cares are unlikely to be necessary. Within the range of the experimental conditions employed, the shrinkage of the spherical sample was less than 2 to 3 percents of the initial diameter.

In the case of the slab sample, the shrinkage of the sample had only a lesser effect. However, it was still necessary for an accurate measurement to bond the bead of the thermocouple to the sample at a fixed position.

The thermocouple employed was a chromel-alumel thermocouple of 0.1 to 0.3 mm in diameter, and the number of the temperature measurement positions was two or three for the spherical sample and six for the slab sample.

4. 2. 4. Determination of Conversion

The conversion of the spherical sample was determined from the relation between the measured weight decrease and time according to the following equation:

$$k=(w_i-w)/(w_i-w_e)$$

where w_i and w_e denote the initial weight and the weight at the equilibrium, respectively. The sample weight measured at the equilibrium was in a quite good agreement with that calculated from the stoichiometric relation of the reaction. Therefore, the dehydration of the calcium hydroxide sample employed was considered to be completed irreversibly within the range of the experimental conditions employed. For the slab sample, based on the measured temperature distribution, a local conversion was first calculated from the relation assumed between the conversion and the temperature. Then the conversion of the slab sample was determined by integrally averaging the local conversion calculated.

4. 3. Results and Discussion

4. 3. 1. Measurement and Evaluation of Physical Properites

For the reaction temperature of calcium hydroxide (the equilibrium temperature

of dehydration under an atomospheric pressure) a few measurements have been made previously. Those are: 540℃ by Johnston; *et al.*[16], and 512℃ by Halstead and Moore[17]. If a solid sample is heated from the surroundings at a higher ambient temperature than such an equilibrium temperature under an atomospheric pressure, the effective initial temperature of thermal decomposition of the solid should be almost equal to this equilibrium temperature so long as the diffusion rate of the decomposed gas has no controlling effect. This is mainly because thermal decomposition usually has a relatively large activation energy. As mentioned above, the ambient temperature (the heating temperature) in the present measurement was in the range of 600 to 750℃, being much higher than the equilibrium temperature, and the measured effective initial temperature of dehydration was around 520℃ with a very little scatter dependent on the heating conditions. Thus, the initial reaction temperature was assumed to be 520℃. For the final reaction temperature, there is no established method to be determined. Therefore, applying several values ranged between 525 to 570℃ to the final reaction temperature, a preliminary calculation of Equation (51) and (52) was carried out, and a comparison was made between these results. The differences observed between the results were a relatively little, especially no appreciable differences were observed for the final temperature lower than 540℃. Thus, the final temperature was assumed conventionally to be 540℃ in the present calculation.

For the heat of dehydration, the value, 337 kcal/kg, was applied, which was measured by Halstead and Moore[17] according to the van't Hoff equation. Using this value, the overall specific heat, $C_p(t)$, was calculated as follows;

$$C_p(t)=c_p+H(\partial k/\partial t)$$

or

$$\left.\begin{aligned} C_p(t)&=c_{p1}, \quad t<t_1 \\ C_p(t)&=Kc_{p1}, \quad t_1\leq t\leq t_2 \\ C_p(t)&=c_{p2}, \quad t>t_2 \end{aligned}\right\} \tag{58}$$

where $K=1+H/\{c_{p1}(t_2-t_1)\}$, and t_1, t_2, c_{p1} and c_{p2} denote the initial and the final temperatures of the reaction, the specific heats in the pre- and in the post-reaction states, respectively.

Fig. 16 shows the thermal conductivities in the non-reaction states measured by a hot wire method the applicabilities of which have been demonstrated in Section 3, in the ranges of the temperatures between 100 and 400℃ for the calcium hydroxide samples, and between 200 and 750℃ for the calcium oxide samples, respectively. For the thermal conductivity with reaction of calcium hydroxide, the measured ratio, Λ/λ_1, (λ_1: the thermal conductivity in the pre-reaction state) is 0.25 ± 10 % as shown in Table 10.

For the specific heats and densities, the respective constant value was applied to each of the reaction states, since the temperature dependencies of these quantities are usually small, compared with that of a thermal conductivity.

The gray emissivity of the sample, ε_s, was calculated from the spectral emissivity data of calcium oxide, ε_λ, according to the following integration:

$$\varepsilon_S = \int_0^\infty \varepsilon_\lambda E_\lambda(T_S) d\lambda / \sigma T_S^4$$

The spectral emissivity of calcium oxide was measured at about 600 ℃ by the Double Beamed Null Method in the range of the wave-lengths between 1.0 and 15.0 μm, and the result is shown in Fig. 17. Using the gray emissivity thus obtained, the overall gray absorptivities of radiation were evaluated as follows:

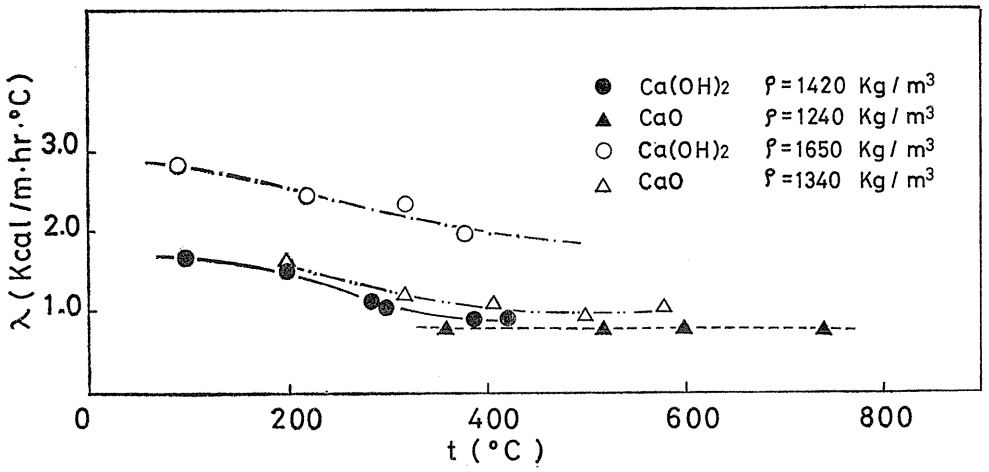

Fig. 16. Thermal conductivities of calcium hydroxide and calcium oxide measured by a hot wire method (non-reaction state).

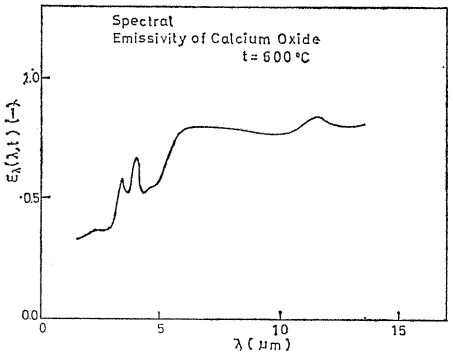

Fig. 17. A spectral emissivity data of calcium oxide measured at 600 ℃.

(For a spherical sample)

$$\phi_{S-W} = 1/\{(1/\varepsilon_S) + (D_S/D_W)^2(1/\varepsilon_W - 1)\} \tag{59}$$

(For a slab sample)

$$\left.\begin{aligned} \phi_{S-W} &= 1/\{(1/\overline{F}_{S-W}) + (1/\varepsilon_W - 1) + (1/\varepsilon_S - 1)\} \\ \overline{F}_{S-W} &= F_{S-W} + F_{S-W} \cdot F_{R-W}/(1 - F_{R-R}) \end{aligned}\right\} \tag{60}$$

where F denotes a geometric factor of radiation.

The natural convection heat transfer coefficient was evaluated from the equation reported by Yuge[18] for the spherical sample and neglected for the slab sample.

4. 3. 2. Unsteady Temperature Distribution in a Solid Sample

Figs. 18 to 20 show examples of comparisons between the experimental data

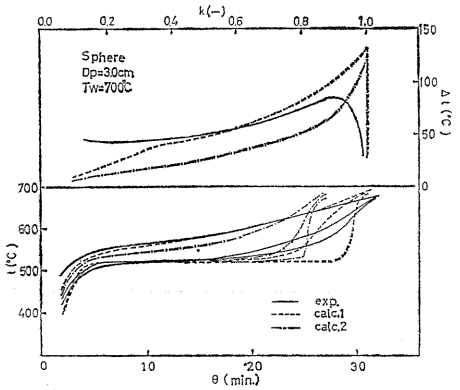

Fig. 18. A comparison between the experimental data and the calculated results of the unsteady temperature distribution (for a spherical sample).

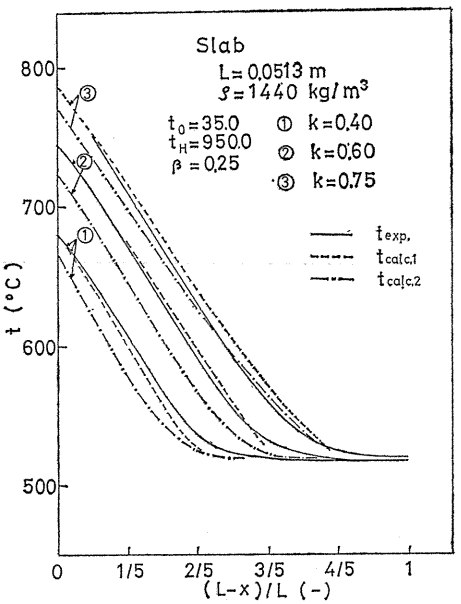

Fig. 19. A comparison between the experimental data and the calculated results of the unsteady temperature distribution (for a slab sample).

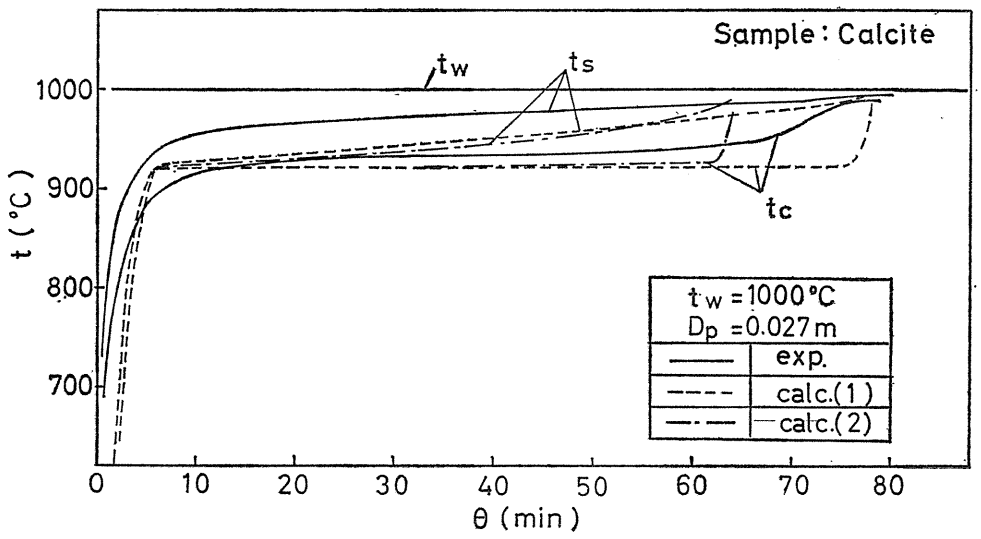

Fig. 20. A comparison between the experimental data[19] and the calculated results for a calcite sphere.

and the calculated results of the unsteady temperature distribution in a solid sample. Figs. 18 and 19 show those in a spherical and a slab samples, respectively, and Fig. 20 shows that in a spherical calcium carbonate (a calcite) sample the experimental work of which was carried out in the author's previous work[19], and the physical properties employed of which are shown in Table 12.

Table 12. Physical properties of a calcite and CaO formed by the reaction.

Sample	H (kcal/kg)	$c_p(t)$ (kcal/kg ℃)	$\rho(\varepsilon)$ (kg/m^3)	λ_e (kcal/m hr ℃)	A (kcal/m hr ℃)
$CaCO_3$	426.0	0.31 (900℃)	2710 (0.0)	2.30 (900℃)	0.64～0.69 (900～920℃)
CaO		0.23 (900℃)	1740 (0.48)	1.00 (900℃)	

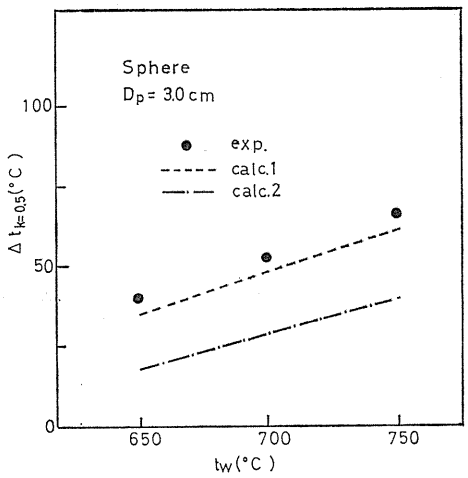

Fig. 21. Temperature differences between the surface and the center of a calcium hydroxide sphere at $k=0.5$.

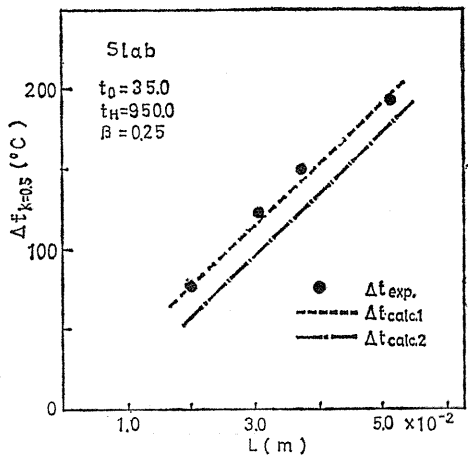

Fig. 22. Temperature differences between the upper and the lower surfaces of a calcium hydroxide slab at $k=0.5$.

In this kind of heat transfer problem, the maximum temperature difference produced in the solid is also a good measure to discuss its characteristics. In Figs. 21 and 22, the maximum temperature differences at the fixed conversion, $k=0.5$, are plotted against the heating temperature (for a spherical sample) or the thickness of a sample disc (for a slab sample).

As is seen from Figs. 18 to 22, the following experimental trends (denoted by a solid line in the figures) were obtained within the range of the experimental conditions employed: (1) both the temperatures at the center of the spherical sample and on the lower surface of the slab sample remain the nearly constant value equal to the initial reaction temperature of the reactant (about 520 ℃ for calcium hydroxide and about 900 ℃ for a calcite) throughout the whole period excepting the initial and the final stages of the reaction, and (2) the maximum temperature difference produced in the sample during the reaction increases with

the increases in the conversion, the heating temperature and the radius or thickness of the sample.

These experimental trends are also in fairly good agreements with both the trends observed from the results of the 'calc. 1' (denoted by a dotted line) and from those of the 'calc. 2' (denoted by a chained line). Therefore, it would be first concluded that an unsteady heat conduction has a controlling effect on the overall kinetics of an one-stage endothermic solid reaction like the dehydration of calcium hydroxide and the decarbonization of a calcite.

In a comparison between the 'calc. 1' and the 'calc 2', the 'calc 1' was observed to show a better coincidence with the experimental data especially for the maximum temperature difference than the 'calc. 2' within the range of the experimental conditions employed.

4. 3. 3. Dead Time of Reaction

The results of the dead times of the reactions are shown in Figs. 23 and 24. In Fig. 23, the ratios of the theoretical dead times to the experimental ones, $\theta_{calc.}/\theta_{exp.}$, of the dehydration of calcium hydroxide are plotted against the heating

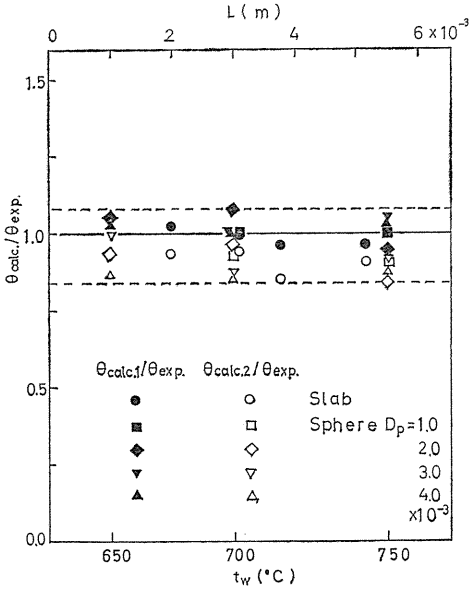

Fig. 23. Comparisons between the calculated and the experimental results of the dead-times of the reaction (for CaO).

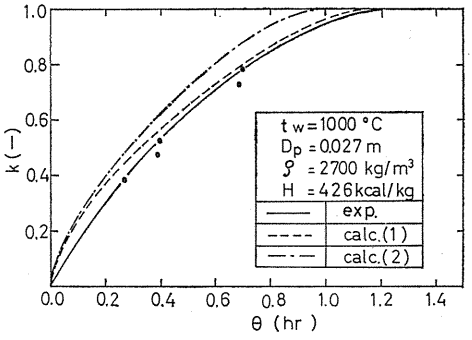

Fig. 24. A comparison between the calculated and the experimental relations of the conversion to time (for a calcite).

temperature (for a spherical sample) or the thickness of a sample disc (for a slab sample). The heating temperature for the slab sample in Fig. 23 is quite the same as that in Figs. 19 and 22. In Fig. 24, comparisons are made between the experimental and the theoretical relations of the conversion to time, obtained under the same condition as that in Fig. 20 for the decarbonization of a calcite. As is seen

from Figs. 23 and 24, within the range of the experimental conditions employed, the results from the 'calc. 1' were also recognized to be in a better agreement with the experimental data than those from the 'calc. 2' for both the dehydration and the decarbonization. However, the difference between the 'calc. 1' and the 'calc. 2' is not so large as that in the case of the temperature distribution. Roughly speaking, a heat flow rate in a solid is, in general, determined by the product of a thermal conductivity and a temperature gradient in a solid. In the 'calc. 1', the thermal conductivity is smaller but the temperature gradient produced in the solid is larger, compared with those in the 'calc, 2'. Therefore, the product of these two quantities would have no large differences between the two cases. This may be a principal reason why the thermal conductivity with reaction has only a smaller effect on the theoretical dead times of the reaction than that on the temperature distributions in the solid sample.

Summing up the above results, it was shown, within the range of the experimental conditions employed, that the theoretical analysis taking account of the thermal conductivity with reaction fitted the problem of an unsteady heat conduction accompanied by an one-stage endothermic solid reaction better than the theory which did not involve an effect of the thermal conductivity with reaction. However, it was also shown that as long as the dead time of the reaction was concerned, the two theories had no large difference.

5. Unsteady Heat Conduction Accompanied by a Two- or a Multi-Stage Endothermic Solid Reaction

In this section, it is aimed to discuss the applicabilities of the overall specific heat and the thermal conductivity with reaction to the problem of an unsteady heat conduction accompanied by a two- or a multi-stage endothermic solid reaction. In a two- or a multi-stage reaction, the reaction kinetics become more complicated and the heat capacity of a solid has a much more serious effect than those in an one-stage reaction. However, if the concept of the overall specific heat is proved to be also applicable to this problem, the mathematical difficulties involved in this problem would be greatly reduced, because the difference between a calculation procedure in a two- or a multi-stage reaction and that in an one-stage reaction is usually very small. In the case of an one- stage reaction, the overall specific heat-temperature relation belongs to the type (a) or the type (b) shown in Fig. 1. On the other hand, in the case of a two- or a multi-stage reaction, in general, either the type (c) or the type (d) is applied to this relation. This may be the largest difference between the two cases.

Again the same type of the basic equation as Equation (9) is applied to the problem of an unsteady heat conduction accompanied by a two- or a multi-stage endothermic solid reaction. If the appropriate physical properties of this reaction system are known as functions of temperature, the basic equation would be solved numerically by a similar method to that in Section 4.

5. 1. Two-Stage Dehydration of Gypsum[1, 20, 21]

5. 1. 1. Modelling of the Overall Specific Heat

As shown before in Fig. 10, in the two-stage dehydration of gypsum, the two

dehydration reactions (one is $CaSO_4 \cdot 2H_2O \longrightarrow CaSO_4 \cdot 1/2H_2O + 3/2H_2O$ and another is $CaSO_4 \cdot 1/2H_2O \longrightarrow CaSO_4 + 1/2H_2O$) usually take place separately in the two quite different regions of the reaction temperatures. In this type of two- (or multi-) stage endothermic solid reaction, therefore, the discussions made for an one stage reaction in Section 4 may be also valid for each of the two reactions, and then the relations between the physical properties and temperature are expressed in the form shown schematically in Fig. 25. Thus,the overall specific heat becomes, in this case,

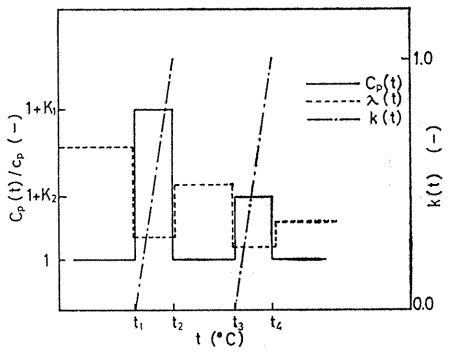

Fig. 25. Illustrative variations of the physical properties for a two-stage endothermic solid reaction.

$$\left.\begin{aligned} C_p(t) &= c_{p1}, \quad t < t_1 \\ C_p(t) &= K_1 c_{p1}, \quad t_1 \leq t \leq t_2 \\ C_p(t) &= c_{p2}, \quad t_2 < t < t_3 \\ C_p(t) &= K_2 c_{p2}, \quad t_3 \leq t \leq t_4 \\ C_p(t) &= c_{p3}, \quad t > t_4 \end{aligned}\right\} \tag{61}$$

where $K_1 = 1 + H_1/\{c_{p1}(t_2 - t_1)\}$ and $K_2 = 1 + H_2/\{c_{p2}(t_4 - t_3)\}$, t_1 and t_2 denote the initial and the final temperatures of the first stage reaction, and t_3 and t_4 denote those of the second stage reaction, respectively. H_1 and H_2 are the heats of the first and the second stage reactions, and c_{p1}, c_{p2} and c_{p3} are the specific heats of $CaSO_4 \cdot 2H_2O$, $CaSO_4 \cdot 1/2H_2O$ and $CaSO_4$, respectively. The other physical properties including the thermal conductivity with reaction have already been shown in Fig. 7, Tables 1 and 3 to 4'. Using these relations and solving numerically Equation (51) with the initial and the boundary conditions, Equation (53), we can obtain a theoretical, unsteady temperature distribution in a spherical gypsum sample, accompanied by the two-stage dehydration.

5. 1. 2. Unsteady Temperature Distribution in a Spherical Sample

Figs. 26 and 27 show typical examples of comparisons between the experimental data and the theoretical results of the unsteady temperature distribution in a spherical sample made of natural gypsum from Africa. In Figs. 26 and 27, the 'calc. 1' and the 'calc. 2' denote quite the same as those in Section 4. As is seen from Figs. 26 and 27, for the two-stage dehydration of gypsum, the same trends as those in Figs. 18 to 20 were also observed in the range of the experimental conditions employed, and the 'calc. 1' was shown to fit also the problem of an unsteady heat conduction accompanied by a two-stage endothermic solid reaction like the dehydration of gypsum better than the 'calc. 1'.

5. 1. 3. Dead Time of Reaction

As has already discussed extensively in Section 4 and also as is seen from

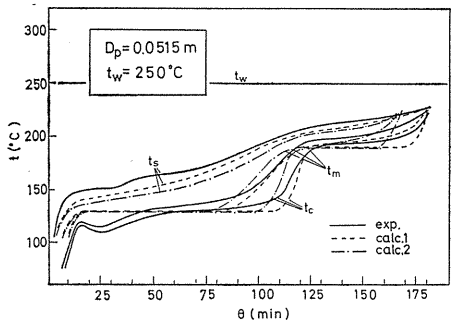

Fig. 26. A comparison between the experimental and the calculated results of unsteady temperature distribution (for a spherical natural gypsum).

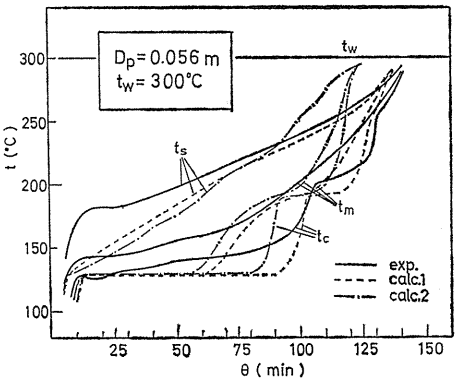

Fig. 27. A comparison between the experimental and the calculated results of unsteady temperature distribution (for a spherical natural gypsum).

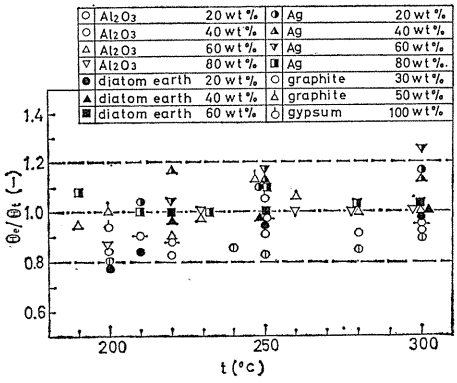

Fig. 28. Effects of the thermal diffusivity, the heat of reaction and the heating temperature on the values, θ_e/θ_t (θ_e; experimental dead-time, θ_t; theoretical dead-time).

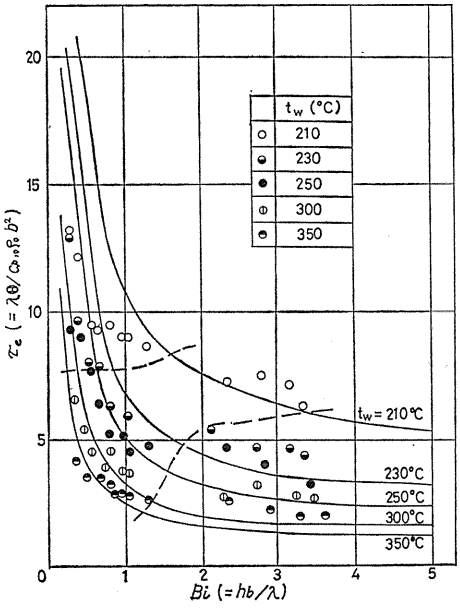

Fig. 29. An effect of the Biot number on the non-dimensional dead time, τ_e.

Figs. 26 and 27, the 'calc. 1' is a better theory than the 'calc. 2'. However, as long as the dead time of the reaction is concerned, in general, there is no serious difference between the two theories. In Figs. 28 and 29, the experimental dead times of the two-stage dehydration of natural- and chemical-gypsum are compared with the theoretical results obtained from the 'calc. 2'. Fig. 28[20] shows the effects of the thermal diffusivity and the heat of reaction of a solid sample employed as well as of the heating temperature on the value, θ_e/θ_t, (e: experimental and t:

theoretical). The thermal diffusivity and the heat of reaction of a solid sample were varied in the ranges shown in Table 13 by mixing chemical gypsum with the inert material like alumina, silver, diatom earth and graphite. In Fig. 29[21] the

Table 13. Physical properties of the chemical gypsum samples mixed with inert materials.

Content of inert material mixed (wt %)		ρ (kg/m^3)	c_p (kcal/kg ℃)	λ (kcal/m hr ℃)	$\alpha=\lambda/c_p\rho$ (m^2/hr)
Al_2O_3	20	1.50 ($\times10^3$)	0.260	0.25	0.64 ($\times10^3$)
	40	1.58	0.248	0.30	0.75
	60	1.60	0.236	0.35	0.93
	80	1.76	0.224	0.39	0.99
Ag	20	1.69 ($\times10^3$)	0.229	0.32	0.83 ($\times10^3$)
	40	2.11	0.189	0.48	1.2
	60	2.74	0.143	0.85	2.2
	80	4.06	0.100	2.00	4.9
Diatom earth	20	1.24 ($\times10^3$)	0.260	0.19	0.59 ($\times10^3$)
	40	1.15	0.240	0.17	0.62
	60	0.97	0.230	0.16	0.72
Graphite	30	1.30 ($\times10^3$)	0.260	0.55	1.6 ($\times10^3$)
	50	1.34	0.250	1.00	3.0
Gypsum		1.44 ($\times10^3$)	0.272	0.20	0.51 ($\times10^3$)

non-dimensional dead times, τ_e, are plotted against the non-dimensional heat transfer coefficients, Bi, (or the Biot number). In this experiment, a natural gypsum sample was immersed in a fluidized bed to vary the heat transfer coefficient in the range between 28 and 290 kcal/m^2. h. ℃. From both Figs. 28 and 29, it is seen that the experimental dead times are in a fairly good agreement with the theoretical results from the 'calc. 2' in the extremely wide range of the experimental conditions employed. Thus, the 'overall specific heat' model was concluded to have also the powerful applicabilities to the problem of a two-stage endothermic solid reaction like the dehydration of gypsum. However, it should be noted that $\theta_{exp.}$ becomes gradually smaller than $\theta_{theo.}$ as the heating rate becomes slower and that $\theta_{exp.}$ becomes larger than $\theta_{theo.}$ as the heating rate becomes higher. These two opposite trends which may limit the applicabilities of the overall specific heat are due to the too rough simplification of intrinsic reaction kinetics in the former case[22] and to the neglect of diffusion of the decomposed gas in the latter case[23], respectively.

5. 2. *Multi-Stage Thermal Decomposition of Coal and Polypropylene*[24, 25]

In the case of a multi-stage (or a continuous) endothermic solid reaction like the thermal decompositions of coal and organic polymers, a key factor is to determine or to model the overall specific heat-temperature relations. Since in these reactions many kinds of a single reaction (perhaps involving a phase change), in

general, take place simultaneously or successively in an extremely complex way, it is difficult to assume the overall specific heat only from a basic reaction kinetic data as in an one-stage or a two-stage reaction. Although a few methods like a differential scanning calorimetry have been reported to discuss the basic reaction kinetics of those thermally decomposing materials, the overall specific heat of those materials, in actual cases, may be affected by the heating rate, the material dimensions and the diffusivities of decomposed gases as well as by the basic reaction kinetics. Therefore, only a conventional method would be available to model the overall specific heat of those materials in engineering applications. For the thermal conductivity with reaction, its determination would be more difficult than that of the overall specific heat.

Again, Equation (51) with the initial and the boundary conditions, Equation (53), is applied to the problem of an unsteady heat conduction accompanied by a multi- (or a continuous) endothermic solid reaction in a spherical sample. Taking a briquet sphere and a sphere of polypropylene-kaolin mixture as samples, the numerical solutions calculated from Epuation (51) are compared with the experimental, unsteady temperature distributions in the samples in Figs. 30 and 31. The physical

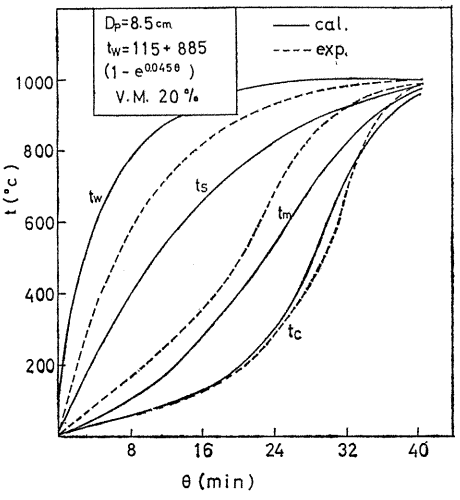

Fig. 30 A comparison between the experimental and the calculated results of the unsteady temperature distribution for a briquet sphere.

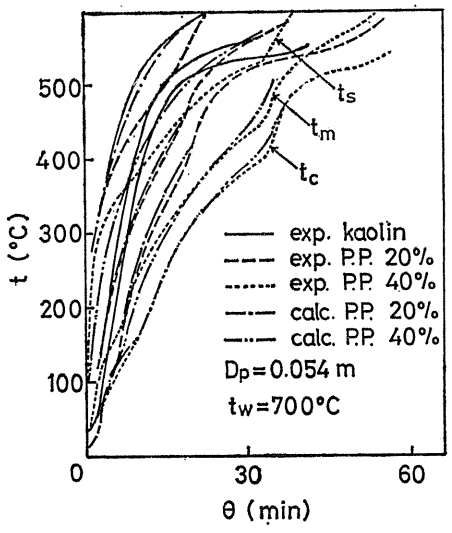

Fig. 31. A comparison between the experimental and the calculated results of the unsteady temperature distribution for a sphere of polypropylene-kaolin mixture.

properties employed in the calculations are: $\lambda=0.94$ kcal/m. h. ℃, $c_p=0.34$ kcal/kg ℃, $\rho=1,300$ kg/m^3 and $\varepsilon_s=0.9$ for a briquet, and the values shown in Table 14 for a polypropylene-kaolin mixture. Of both the samples, Figs. 32 and 33 show the overall specific heats employed, which were modelled by a trial-and-error method. As is seen from Figs. 30 and 31, the 'overall specific heat' model would have basically a powerful applicability to a multi- (or a continuous) endothermic solid reaction, if a more reasonable way is established to model the overall specific heat.

Table 14. Physical properties of the sphere of polypropylene-kaolin mixture.

	thermal conductivity (kcal/m hr ℃)	specific heat (kcal/kg℃)	density (kg/m³)	thermal diffusivity (m²/hr)	melting point (℃)
kaolin	0.8	0.2	1.6×10^{3}	2.5×10^{-3}	
P. P. 20%+kaolin 80%	0.45	0.25	1.2	1.5	
P. P. 40%+kaolin 60%	0.42	0.3	1.1	1.3	
polypropylene	0.10	0.46	0.9×10^{3}	2.4×10^{-4}	164~170

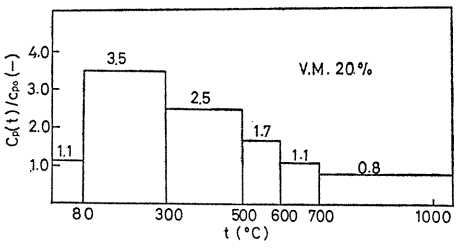

Fig. 32. The overall specific heat of a briquet.

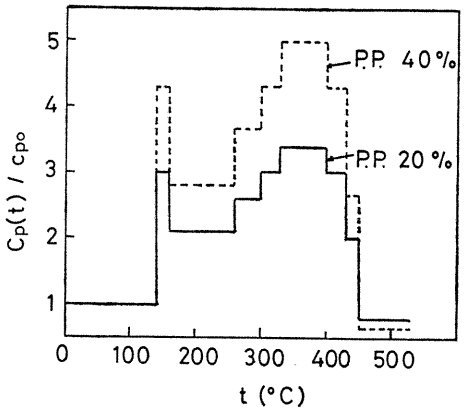

Fig. 33. The overall specific heat of a polypropylene-kaolin mixture.

6. Nomenclature

a = radius of a sample sphere or of a thin wire [m]
b = radius of a cylindrical sample [m]
Bi = Biot number [−]
c_p = specific heat of a sample solid [kcal/kg℃]
$C_p(t)$ = Overall specific heat [kcal/kg℃]
D_p = diameter of a sample [m]
E = monochromatic emissive power [kcal/m²hr]
F = geometric factor of radiation [−]
h = heat transfer coefficient [kcal/m²hr℃]
h_c = natural convection heat transfer coefficient [kcal/m²hr℃]
h_r = radiation heat transfer coefficient [kcal/m²hr℃]
H = heat of reaction per unit mass [kcal/kg]
k = fraction of reaction [−]
K = a constant [−]
l = length of a sample [m]
L = thickness of a slab [m]
Q = heat of reaction per unit volume [kcal/m³]
Q_0 = heat transmitted from the wire per unit volume and unit time [kcal/m³hr]
r = distance from the center of a spherical or cylindrical sample [m]

t = temperature [℃]
Δt = temperature difference [℃]
T = absolute temperature [°K]
w = sample weight [kg]
x = distance from the lower surface of a slab [m]
z = axial distance [m]
α = thermal diffusivity [m^2/hr]
ε = emissivity [−]
θ = time [hr]
θ = dead-time of the reaction [hr]
λ = thermal conductivity of a sample solid [kcal/m hr℃]
Λ = thermal conductivity with reaction [kcal/m hr℃]
ρ = bulk density of a sample solid [kg/m^3]
τ = dimensionless time [−]
ϕ = overall gray absorptivity of radiation (or interchange factor) [−]
σ = Stefan-Boltzmann constant [kcal/m^2hr°K^4]

Subscripts

e = equilibrium
f or 2 = final
i or 1 = initial
m = middle
s = surface or solid
w = wall
λ = spectral

7. References

1) S. Sugiyama and M. Hasatani: Kagaku Kogaku, **28**, 355 (1964).
2) S. Sugiyama and M. Hasatani: *ibid.*, **29**, 158 (1965).
3) K. Nagasaka, M. Shimizu and S. Sugiyama: J. Chem. Eng. Japan, **6**, 264 (1973).
4) W. M. Underwood and R. B. McTaggart: Chem. Eng. Prog., Symp. Series, **56**, 30, 261 (1960).
5) E. F. M. Van der Held and F. G. Van Drunen: Physicia, **15**, 865 (1949).
6) J. H. Blackwell: Can. J. Phys., **31**, 472 (1953), J. Appl. Phys., **25**, 137 (1954), Can. J. Phys., **34**, 412 (1956).
7) H. Matsuda, M. Hasatani and S. Sugiyama: Kagaku Kogaku Ronbunshu, **1**, 589 (1975).
8) H. Matsuda, M. Hasatani and S. Sugiyama: *ibid.*, **2**, 630 (1976).
9) B. M. Mogilevsky and A. Ph. Chundnovsky: Proc. Int. Conf. Phys. Semicond. 9 th, Bd. **2**, 1241 (1968).
10) D. Kunii and J. M. Smith: AIChE J., **6**, 71 (1960).
11) J. E. English and H. E. Rose: Brit. Chem. Eng., **13**, 1135 (1968).
12) J. Francl and W. D. Kingery: J. Am. Ceram. Soc., **37**, 99 (1954).
13) T. Kato, M. Kito, M. Nakamura and S. Sugiyama: Kogyo Kagaku Zasshi, **68**, 94 (1965).
14) M. Kito and S. Sugiyama: Kagaku Kogaku, **28**, 810 (1964).
15) S. Sugiyama and T. Baba: *ibid.*, **28**, 940 (1964).
16) Johnston: Z. Phys. Chem., **62**, 330 (1908).
17) P. E. Halstead and A. E. Moore: J. Chem. Soc., 3873 (1957).
18) T. Yuge: Trans. ASME, Aug. 214 (1960).
19) S. Sugiyama *et al.*: Kagaku Kogaku, **25**, 265 (1961).
20) S. Sugiyama, M. Hasatani and T. Kondo: Kogyo Kagaku Zassi, **69**, 2233 (1966).
21) S. Sugiyama, M. Hasatani and K. Goto: Kagaku Kogaku, **33**, 1276 (1969).

22) S. Sugiyama and M. Hasatani: *ibid.*, **30**, 734 (1966).
23) S. Sugiyama, M. Hasatani and T. Kondo: *ibid.*, **31**, 806 (1967).
24) S. Sugiyama, K. Nagasaka and M. Hasatani: *ibid.*, **30**, 165 (1966).
25) A. Sato, S. Sugiyama and M. Hasatani: *ibid.*, **37**, 51 (1971).

8. Acknowledgement

The authors wish to express their thanks to Drs. M. Nakamura, N. Arai and Mr. H. Matsuda for their helpful cooperations in carrying out the theoretical and the experimental works. They also wish to express their thanks to Prof. M. Shimizu (Tokyo University of Agriculture and Technology), Dr. M. Kuroda (Gumma University), Mr. K. Nagasaka (Aichi Institute of Technology) and Dr. A. Sato (Chubu Institute of Technology) for their instructive discussions.

This work was partly supported by the Grant in Aid of Scientific Research from the Ministry of Education.